Feasibility of Unwaxed and Waxed Banana (*Musa acuminata x balbisiana*) Pseudostem Fibers as Alternative Dental Floss Material

Marianne Loren P. Celedonio, Nicole R. Arguelles, Mohit J. Amarnani,
Katelynn L. Cancio, Maxine H. Darvin, Alyssa Pauline C. Esmabe,
Allen Andrei R. Makasakit, Ailyn B. Anglo–Ojeda, and Fritz M. Ferran
De La Salle Santiago Zobel School - Vermosa Campus, Imus City, Cavite

Abstract: Oral health, waste management, and sustainability are prevalent issues faced by developing countries. Relative to these concerns, there remains a need for oral hygiene essentials that are both effective and environmentally responsible. This study aims to explore the feasibility of banana pseudostem fibers (BPF) as an alternative material for sustainable dental floss in terms of two physical properties, namely, tensile strength and elongation at break. Fibers were mechanically extracted from the outermost sheaths of banana pseudostems to produce two sample groups, unwaxed BPF and waxed BPF, the latter comprising fibers that were coated with a mixture of two parts coconut oil and one part candelilla wax. Both sample groups were tested for tensile strength and elongation at break. According to the mean and SD of both groups and one-way MANOVA, unwaxed BPF had significantly higher tensile strength and elongation at break than waxed BPF, revealing that the wax coating process diminished the physical properties of the BPF due to thermal degradation. Furthermore, the application of the coconut oil-candelilla wax coating was found to have a large effect on tensile strength and a small effect on elongation at break. Results show that there is potential in BPF to be an alternative material for dental floss in relation to the examined properties, although it may not be a substitute for synthetic dental floss material by itself. Modifying the fiber extraction and wax coating processes involved and assessing the chemical properties of the material are also recommended for further research.

Key Words: banana pseudostem fibers; candelilla wax; coconut oil; dental floss; sustainability

1. INTRODUCTION

Oral hygiene is a common problem amongst the youth, and the issue is amplified among those in rural areas. One study explores oral health perceptions and dental care behaviors among such rural adolescents, enumerating several difficulties regarding dental care access such as finances, transportation, fear, issues with health insurance, and parental responsibility (Dodd et al., 2014). The aforementioned factors that impede the attainment of good oral health are further augmented in the case of low-income communities in poor developing countries. Many of these communities do not have sufficient income to acquire oral health, nor do they have immediate access to such.

A greater extent of knowledge on oral health promotion was equated to a greater frequency of tooth brushing and dental flossing (Akpabio et al., 2008). Even then, most oral hygiene essentials such as toothbrushes and dental floss make use of plastic, which has constantly been reported to be dangerous not just to the environment but also to human health. While some studies and inventions attempted to develop commercially sold oral hygiene essentials into more sustainable commodities, most of the resulting products only partially consist of biodegradable materials. Hence, the purpose of this study is to explore possible alternative materials that may be used in creating an oral hygiene essential that is not only completely biodegradable but can also be produced through sustainable methods.

2. LITERATURE REVIEW

Dental floss or dental tape is one of the commonplace instruments used in oral hygiene. At its simplest, it is a filament (or a bundle of filaments) that fits between two teeth for the removal of material. Burch (1995) states that the tensile strength of dental floss significantly affects its durability and efficacy. To reduce the risk of gum injury from flossing, some variants of dental floss are coated with wax to decrease the coefficient of friction. Submergence techniques are commonly employed to ensure that each fiber is evenly coated. Following this, the excess coating is removed, and the floss threads are dried to solidify the wax coating and prevent contamination

(Tseng et al., 2000). Standard dental floss waxing usually requires a wax that has a melting point between about 57°-93°C, such as beeswax, paraffin, candelilla, and microcrystalline waxes (Evazynajad & LeGrande, 2006).

Most studies geared toward the development of sustainable dental floss have utilized silk as the raw material, while others modified the components of the wax coating instead of the floss material itself. Table 1 displays a summarized comparison among several forms of dental floss.

Table 1. *Comparison of Dental floss from other Studies*

Author	Dental floss material	Tensile strength (N)	Elongation at break (%)
Phonhan et al., 2014	Thai silk (Nang noi), waxed	15.65	28.5
Supanitayanon et al., 2017	synthetic (nylon), unwaxed	47.39	31.25
	synthetic (nylon), waxed	46.46	44.62
	Thai silk, waxed	23.70	16.44
Suwansanit, 2009	synthetic[a]	2.56–50.70	7.69–53.96
	Thai silk, unwaxed	24.2 ± 6.5	11.5 ± 1.7
	Thai silk, waxed	20.4 ± 2.8	23.9 ± 7.0
Tseng et al., 2000	synthetic	14.61–32.56	N/A

a. *From seven kinds of commercial dental floss*

Banana fiber is a lignocellulosic fiber, which is obtained from the pseudostem of banana plants. Banana fiber has good strength properties comparable to those of conventional materials such as glass fiber. It is lightweight and sustainable and has a high level of strength, smaller elongation, and better fire resistance (Bhatnagar et al., 2015). In terms of fiber extraction and processing, Subagyo and Chafidz (2018) identified three main steps: 1) tuxing, which refers to the manual or mechanical removal of the fiber bundles from the pseudostem layers; 2) retting, which involves water absorption and microbial activity to decompose pectin, the substance which binds the fibers to the woody center of the pseudostem, and; 3) degumming, which entails the boiling and washing of fibers to neutralize them, remove impurities, and break them down into smaller filaments (Ebisike et al., 2013).

From reviewing existing literature, the proposed product is a wholly sustainable alternative material for dental floss made primarily out of banana pseudostem fibers (BPF) and coated with a natural wax.

3. CONCEPTUAL FRAMEWORK

As shown in Figure 1, the research involves one independent variable: the application of the coconut oil-candelilla wax coating. Additionally, two dependent variables represent physical properties to be measured: 1) tensile strength and 2) elongation at break.

Previous studies have demonstrated that

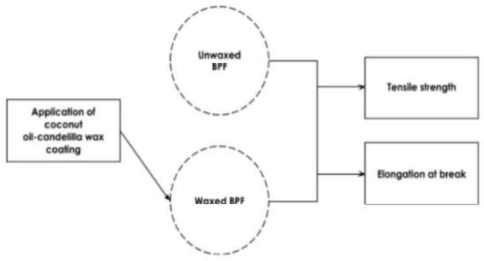

Figure 1. *Diagram of Conceptual Framework*

plant fibers are a feasible alternative raw material for dental floss in terms of physical properties. The most relevant of these properties are tensile strength and elongation at break, which are both thoroughly associated with dental floss efficacy. Among several natural fibers, the intrinsic physical characteristics of BPFs—which the chemical compounds cellulose and lignin are responsible for—make them ideal substitutes to synthetic polymers such as nylon (Subagyo & Chafidz, 2018) and, therefore, appropriate for the experimental dental floss material. However, a certain intervention is required to improve the elongation of banana fibers.

According to Suwansanit (2009), the presence of a wax coating can significantly increase the elongation of dental floss. The utilization of BPF for the experimental dental floss material in this study leads the researchers to assume that the effect of a wax coating on dental floss might also be applicable to plant fibers, at least in part. Hence, the application of a wax coating will be the intervention done on BPF to increase their elongation at break and, at the same time, emulate the components found in standard dental floss. In addition, coconut oil and candelilla wax are the chosen wax mixture ingredients for these reasons: their antimicrobial properties (Peedikayil et al., 2015), their average melting point that meets the minimum requirement for dental floss wax, and their recurrent use in both experimental and commercially available dental floss as a substitute for synthetic waxes.

4. STATEMENT OF THE PROBLEM

1. What is the effect of the utilization of banana pseudostem fibers (BPF) and the application of the coconut oil-candelilla wax coating on the tensile strength and elongation at break of the unwaxed and waxed BPF?

2. Is there a significant difference in tensile strength and elongation at break between the unwaxed BPF and waxed BPF?

5. METHODOLOGY

This study utilized an experimental research design comprising two sample groups: 1) unwaxed

BPF or manually extracted banana pseudostem fibers and 2) waxed BPF or manually extracted banana pseudostem fibers coated with the coconut oil-candelilla wax.

Banana pseudostems and coconuts were procured from a local farm and market. Candelilla wax was purchased from a cosmetics supplier. Other necessary materials were provided by the researchers to account for the unavailability of laboratories. A research ethics checklist and request letter for data gathering were also submitted for permission to conduct the methods at home.

The outer sheaths were separated from the inner layers of the pseudostem by hand. For each sheath, the non-fibrous internal layer was pulled from the fibrous external layer with a knife. The trimmed fibrous layers were boiled for 45 minutes then repeatedly scraped to be separated into individual strands. These fibers were washed with distilled water and left to dry overnight. After, the fibers were randomly grouped into two, corresponding to the two sample groups—unwaxed BPF and waxed BPF. Then, oil was extracted from fully mature coconuts using the hot extraction method (Agarwal & Bosco, 2017). The coconut oil was mixed with candelilla wax in the ratio 2:1, respectively, and heated through a bain-marie at 80°C. Fibers for the waxed BPF group were immersed in the heated wax mixture, then transferred one by one to a parchment-lined tray. Finally, samples were packaged and delivered for testing through the ASTM D 3822 method.

Data were later organized in Excel prior to statistical treatment.

6. DATA ANALYSIS

Data were analyzed through mean and standard deviation comparison and one-way MANOVA with the aid of IBM SPSS Version 24 software.

7. RESULTS AND DISCUSSION

7.1 Effects of BPF utilization and wax application on the physical properties of the experimental dental floss material

Sixty-four cases were examined for each group (n=64). As seen in Table 2, unwaxed BPF has higher tensile strength (M = 11.96, SD = 3.52) than waxed BPF (M = 4.63, SD = 1.54). Similarly, the elongation at break of unwaxed BPF (M = 3.77, SD = 0.73) is higher than that of waxed BPF (M = 3.01, SD = 1.35).

Both unwaxed and waxed BPF possess lower tensile strength and elongation compared to most commercially sold dental floss, as well as experimental dental floss from previous studies.

Table 2. *Descriptives*

Material for Sustainable Dental Floss (BPF)	n	Tensile Strength (N)		Elongation at Break (%)	
		M	SD	M	SD
unwaxed BPF	64	11.96	3.52	3.77	0.73
waxed BPF	64	4.63	1.54	3.01	1.35

Remarks: Mean tensile strength and elongation at break only describe the physical properties of the samples and are not indicative of their possible effects on users (e.g. regarding safety, preference).

Frequently exposing the fibers to water during the extraction procedures may have reduced fiber extension (Subagyo & Chafidz, 2018). A multicomponent polymer dental floss developed by Tseng et al. (2000) had a break strength in the range of 14.61–32.56 N, the minimum value of which is relatively close to the unwaxed BPF's mean tensile strength of 11.96 N. What makes this comparison interesting is that the polymer dental floss and unwaxed BPF have nearly similar tensile strengths despite the former comprising synthetic material and a larger number of filaments than the latter, suggesting that there are merits to unwaxed BPF.
Statistical analysis shows that unwaxed BPF had better tensile strength and elongation at break than waxed BPF, which indicates that the application of the coconut oil-candelilla wax coating had an adverse effect. This is contrary to what was previously believed, particularly that the wax would significantly improve elongation (Supanitayanon et al., 2017; Suwansanit, 2009). A primary reason for the negative effect of the wax application may be the thermal degradation of BPF, which takes place at 30–144°C. Submerging the fibers at a temperature of 80°C during the wax coating process led to physical deterioration due to the evaporation of moisture from the fibers (Alwani et al., 2014, as cited in Subagyo & Chafidz, 2018).

7.2. Feasibility of unwaxed and waxed BPF as an alternative dental floss material

Table 3. *Multivariate Tests and Test Between-Subjects Effects*

Effect		Value	F	Hypothesis df	Error df	Sig.	Partial Eta Squared[d]
Group: Unwaxed and waxed BPF	Pillai's Trace	.649	115.572	2.000	125.000	.000	.649
	Wilks' Lambda	.351	115.572	2.000	125.000	.000	.649

Dependent Variable	Type III Sum of Squares	df	Mean Square	F	Sig.	Partial Eta Squared[d]
Tensile Strength	1719.911	1	1719.911	232.790	.000	.649
Elongation at Break	18.369	1	18.369	15.665	.000	.111

a. *Design: Intercept + unwaxed and waxed BPF*
b. *Exact statistic*
c. *Each F tests the multivariate effect of Group. These tests are based on the linearly independent pairwise comparisons among the estimated marginal means.*
d. *Partial eta squared can be cited as a measure of effect size: f2 is Cohen's effect size: .02 = small, .15 = moderate, .35 = large.*

Table 3 presents a significant difference in tensile strength and elongation at break between unwaxed and waxed BPF $F(2, 125) = 115.572$, $p < 0.05$, Pillai's Trace = 0.649, partial 2 = 0.649. Furthermore, the application of the coconut oil-candelilla wax coating had a large impact on tensile

strength (partial 2 = 0.649) and a small effect on elongation at break (partial 2 = 0.111).

Results correspond with those of Phonhan et al. (2014) despite varying floss material, although few works offer justification. In this study, at least, it can be inferred that the discrepancies in data are not solely a consequence of the wax application but are also attributed to the intrinsic physical characteristics of BPF. Jayaprabha et al. (2011) found that banana fibers across various pseudostem layers differed far more in maximum force sustained than they did in elongation, hence the larger discrepancy in tensile strength and the smaller discrepancy in elongation between the two BPF samples. Nonetheless, theoretical explanations must be considered, as the experiment is only limited to two physical properties. It is possible that what the waxed BPF samples lack in physical properties is compensated for in other areas such as user experience, refined fiber surface (Supanitayanon et al., 2017; Reddy & Yang, 2005), and antimicrobial properties (Peedikayil et al., 2015; Darby & Walsh, 2010).

In light of existing literature, it can be deduced that the less favorable physical properties of waxed BPF are not necessarily a consequence of the wax coating itself, but rather of the process by which the wax was applied to the fibers. On its own, BPF may not be a suitable substitute for conventional dental floss material and would need to be supplemented with some sort of synthetic ingredient or treatment to meet the criteria for standard dental floss. Even so, it is safe to conclude that when met with the exact conditions provided by the research, there is potential for BPF to be further developed into an alternative material for dental floss that is not only on par with conventional materials but is also sustainable and environment-friendly.

8. CONCLUSIONS

In summary, unwaxed BPF possesses significantly higher tensile strength and elongation at break than waxed BPF. The adverse effect of the wax application on the physical properties of the BPF is not necessarily because of the wax itself, but rather of the wax coating process employed, wherein exposure to a certain temperature led to the thermal degradation of the fibers. Information derived from existing literature shows that, while unwaxed BPF has better physical properties, waxed BPF is not entirely unfeasible due to the added benefits provided by the application of wax. By itself, BPF may not be a suitable replacement for commercially available dental floss, but modifying the processes involved in this research may further develop BPF into a comparable and sustainable alternative to conventional dental floss material. It is worth noting, though, that the scope of this discussion is limited, as it only entails two physical properties for variables. For future studies, combining banana fibers with another synthetic or natural ingredient and developing banana fiber-derived plastics may lead to more feasible products. Analyzing chemical and antimicrobial properties is also recommended.

9. ACKNOWLEDGMENTS

We are thankful to Mr. Gerald Gamboa for being one of our statistical consultants and Ms. Airah Marie Valles for helping us refine the structural and grammatical aspects of this paper. We would also like to express our immense gratitude to the Philippine Textile Research Institute (DOST-PTRI) for extending its services to us during the data gathering process.

10. REFERENCES

Agarwal, R. K., & Bosco, S. J. D. (2017). Extraction processes of virgin coconut oil. MOJ Food Processing & Technology, 4(2), 00087.

Akpabio, A., Klausner, C. P., & Inglehart, M. R. (2008). Mothers'/guardians' knowledge about promoting children's oral health. American Dental Hygienists' Association, 82(1), 12.

Bhatnagar, R., Gupta, G., & Yadav, S. (2015). A review on composition and properties of banana fibers. Cellulose, 60, 65.

Bourgeois, D. M., & Llodra, J. C. (2014). Global burden of dental condition among children in nine countries participating in an international oral health promotion programme, 2012–2013. International Dental Journal, 64, 27-34. https://doi.org/10.1111/idj.12129.

Burch, R. R. (1995). Dental floss based on robust segmented elastomer (U.S. Patent No. 5,433,226). Washington, DC: U.S. Patent and Trademark Office. https://patents.google.com/patent/US5433226A/en.

Darby, M.L. and Walsh, M. (2010). Dental hygiene: Theory and practice. Elsevier.

Dodd, V. J., Logan, H., Brown, C. D., Calderon, A., & Catalanotto, F. (2014). Perceptions of oral health, preventive care, and care-seeking behaviors among rural adolescents. Journal of School Health, 84(12), 802-809. https://doi.org/10.1111/josh.12215.

Ebisike, K., AttahDaniel, B. E., Babatope, B., & Olusunle, S. O. O. (2013). Studies on the extraction of naturally-occurring banana fibers. The International Journal of Engineering and Science, 2(9), 95-99.

Evazynajad, A., & LeGrande, W. E. (2006). Dental floss coated with soywax (U.S. Patent Application No. 11/204,453). https://patents.google.com/patent/US20060118131A1/en.

Jayaprabha, J. S., Brahmakumar, M., & Manilal, V. B. (2011). Banana pseudostem characterization and its fiber property evaluation on physical and bioextraction. Journal of Natural Fibers, 8(3), 149–160. doi:10.1080/15440478.2011.601614.

Peedikayil, F. C., Sreenivasan, P., & Narayanan, A. (2015). Effect of coconut oil in plaque related gingivitis—A preliminary report. Nigerian Medical Journal: Journal of the Nigeria Medical Association, 56(2), 143. https://dx.doi.org/10.4103%2F0300-1652.153406.

Phonhan, C., Yangyuen, S., & Wongkasem, S. (2014). The Design and Development of Machine for Producing the Natural Dental Floss. Procedia Engineering, 69, 751-757. https://doi.org/10.1016/j.proeng.2014.03.051.

Reddy, N., & Yang, Y. (2005). Biofibers from agricultural byproducts for industrial applications. Trends in Biotechnology, 23(1), 22-27. https://doi.org/10.1016/j.tibtech.2004.11.002.

Rojas-Molina, R., De León-Zapata, M. A., Saucedo-Pompa, S., Aguilar Gonzalez, M. A., & Aguilar, C. N. (2013). Chemical and structural characterization of Candelilla (Euphorbia antisyphilitica Zucc.). Journal of Medicinal Plants Research, 7(12), 702-705. https://doi.org/10.5897/JMPR11.321.

Subagyo, A., & Chafidz, A. (2018). Banana pseudo-stem fiber: Preparation, characteristics, and applications. In Banana Nutrition-Function and Processing Kinetics. IntechOpen. doi:10.5772/intechopen.82204.

Supanitayanon, L., Dechkunakorn, S., Anuwongnukroh, N., Srikhirin, T., Roongrujimek, P., & Tua-ngam, P. (2017). Mechanical and physical properties of various types of dental floss. Key Engineering Materials, 730, 155-160. https://doi.org/10.4028/www.scientific.net/KEM.730.155

Suwansanit, T. (2009, September 23). Physical properties of dental floss made from Thai natural silk [Poster session]. 2009 Asia/Pacific Region Meeting, Wuhan, China. https://iadr.abstractarchives.com/abstract/papf09-125132/physical-properties-of-dental-floss-made-from-thai-natural-silk.

Tseng, M. M., Masterman, T. C., Park, E. H., Roberts, M. F., & Spencer, J. L. (2000). Dental floss (U.S. Patent No. 6,027,592). Washington, DC: U.S. Patent and Trademark Office. https://patents.google.com/patent/US6027592A/en.

Hybrid Pigments Based on Anthocyanins and Clay Minerals: A Mini Review

Greg Antonio O. Abines, Noah H. Bernardo, Gwyneth Venice S. Santos, and Kathleen O. Tesalona
De La Salle University Integrated School, Manila

Abstract: The synthesis of hybrid pigments has been studied as these provide a safer alternative to modern synthetic pigments that are stable but are unsafe. This paper provides a systematic review of previous research on hybrid pigments composed of anthocyanins combined with different mineral clays, particularly saponite, montmorillonite, halloysite, palygorskite, and sepiolite. The research was carried out by summarizing the related literature cited and comparing each paper to another by the processes that were used and interactions that occurred in creating the hybrid pigment. The findings showed that the literature cited used adsorption as the method of combining the anthocyanin dye and the mineral clays used; the interactions that occurred were the intercalation of the dye and stabilizer used. Additionally, it was shown that the hybrid pigments exhibited improvement with respect to their stability in different areas, particularly pH, chemical, thermal, color, and light stability. Overall, the paper has shown the development and improvement in hybrid pigment research, particularly with anthocyanin hybrid pigments.

Key Words: hybrid pigments; anthocyanins; clay minerals

1. INTRODUCTION

Pigments have played an important role in multiple industries, particularly the food, automotive, plastic, and paint industries (Bruni et al., 2019). Natural pigments are organic pigments derived from organic sources such as plants, animals, and fungi (Dufosśe, 2014). These plant-based natural dyes and pigments are useful but are unstable, meaning they are susceptible to fading and possess poor colorfastness (Kasiri & Safapour, 2013). Synthetic inorganic pigments are used in different applications across different industries for their incredible stability, although their disadvantage is their toxicity (Venil & Lakshmanaperumalsamy, 2009). With these in mind, the synthesis of hybrid pigments has been studied as hybrid pigments are a combination of the qualities of both organic and inorganic materials.

In order for a hybrid pigment to be produced, a natural pigment source will have its dye extracted through different methods. After the dye is extracted, another set of processes is done to combine the dye and the inorganic material, such as a binder or a stabilizer. It is incorporated into the composition of the pigment to improve the quality of the colorant, making a hybrid pigment in the process (Li et al., 2019). Current research papers have shown different results depending on the materials used and the processes involved in creating the hybrid pigment.

The information produced by each paper contributes to the existing body of knowledge regarding hybrid pigments, although papers which summarize these research papers for convenience are not common. The research gap presents itself, as there is a need for organized information and knowledge regarding hybrid pigments. This paper aims to summarize past research regarding the production of hybrid pigments and discuss the processes, chemical interactions, and results of the cited literature.

As discussed, organic pigments are environmentally friendly and safe to use compared to inorganic pigments that are more stable but harmful. Hybrid pigments are created to combine the stability and safety of both, although there is a lack of organized information regarding hybrid pigments. The objective of this research is to address the following research statements:

a) Identify past research that discusses hybrid pigments created with anthocyanins and different stabilizers.
b) Determine the processes and chemical interactions brought about by the experimentation.
c) Compare the pigments produced based on the processes, safety, and stability given the information gathered from past research.

The paper discusses different research done in the past regarding hybrid pigments, which will involve the combination of a dye or colorant, specifically anthocyanin, stabilizers including saponite, montmorillonite, halloysite, palygorskite, and sepiolite. The paper will only cover descriptions of

the materials, processes involved in creating hybrid pigments, interactions between the anthocyanin and the stabilizer, and results from each of the experiments performed. The research will be done to help gather the existing knowledge into one paper which would serve as a review of literature for the research papers used and cited. This would help add convenience to future researchers, as the summary paper will help provide the necessary information needed by the researchers to gain a better understanding of hybrid pigments, particularly those made using anthocyanin as the dye material and stabilizers previously mentioned.

2. COMPARISON RESEARCH

The research was carried out by gathering and summarizing multiple research papers regarding hybrid pigments specifically made with anthocyanin dyes and clay minerals such as saponite, montmorillonite, halloysite, palygorskite, and sepiolite. The papers were sourced from different articles and journals from websites such as Google Scholar, ResearchGate, and ScienceDirect.

Anthocyanins were chosen due to their versatility in a variety of applications as well as their abundance in the environment. These compounds exhibit the potential as better industrial colorants, health supplements, and as a component in the development of solar-based, renewable energies (Silva et al., 2017). Singh et al. (2018) cite that anthocyanins are extracted from numerous sources, including flowers, fruits, vegetables, and leaves, thus being a renewable resource.

The clay minerals used were chosen based on the availability of papers that used anthocyanin dyes in creating the hybrid pigment. According to Trigueiro et al. (2018), clay minerals have layered structures and are capable of ion exchange, thus being useful as stabilizing agents for anthocyanins. The ion exchange capacity contributes to the intercalation process with the help of intermolecular forces. The research studies cited were compared to each other by determining the process used in combining the dye and stabilizer, the interactions that occurred, as well as the characteristics of the pigment produced and its applications.

Table 1. *Summary of Cited Research based on Processes Used and Interactions*

Hybrid Pigment	Stabilizer (Reagents Used)	Processes Used	Interactions	Researchers
(1) anthocyanin-saponite	modified saponite (saponite + cetyltrimethylammonium bromide (CTAB))	Adsorption	Intercalation	Lima, Castro-Silva, Silva-Filho, Fonseca, & Jaber (2020)
(2) anthocyanin-saponite	modified saponite (deionized water + hydrofluoric acid + sodium acetate + magnesium acetate tetrahydrate + basic aluminum acetate + silica)	Adsorption	Intercalation	Lima, Silva, Silva-Filho, Fonseca, Zhuang, & Jaber (2020)
(3) anthocyanin-saponite	synthetic saponite (methanol + hydrochloric acid)	Adsorption	Intercalation	Ogawa, Takee, Okabe, & Seki (2017)
(4) anthocyanin-montmorillonite, anthocyanin-halloysite	montmorillonite and halloysite	Adsorption	Intercalation	Li, Mu, Wang, Kang, & Wang (2019)
(5) anthocyanin-montmorillonite	montmorillonite	Adsorption	Intercalation	Ribeiro, Oliveira, Brito, Ribeiro, Souza, Filho, & Azeredo (2018)
(6) anthocyanin-palygorskite	palygorskite	Adsorption	Intercalation	Li, Ding, Mu, Wang, Kang, & Wang (2019)
(7) anthocyanin-sepiolite	sepiolite	Adsorption	Intercalation	Silva et al. (2019)

Table 1 shows a summary of the different research papers cited in this paper. It is noted that several reagents mentioned in the table are modified versions of existing clay minerals to improve the quality of the hybrid pigment further. Adsorption, a process in which a dye and stabilizer solution is centrifuged and left out to dry for the dye to adhere to the stabilizer's surface, is the method commonly used in the cited studies to combine the anthocyanin pigment with the stabilizers (Britannica, 2013). This was the chosen method as clays have high adsorption capacity and are capable of ion-exchange (Trigueiro et al., 2018). The adsorption process, despite being done with different clay minerals, exhibited the same interaction throughout. As explained in a paper by Lagaly, Ogawa, and Dékány (2012), intercalation occurs when molecules from a compound penetrate another compound's layers. In this case, the anthocyanin dyes intercalated into the mineral clays' layers in each of the respective research to form hybrid pigments. Dipole forces attract both the dye and clay together, causing deformation in the interlayers by slowly widening the space between two clay layers. Once the space is large enough, the rest of the dye molecules enter the interspace, combining with the clay and forming a hybrid pigment.

Table 2. *Summary of Cited Research based on Characteristics, Color, Stability, and Application of Pigments*

Hybrid Pigment	Characteristics of Pigment	Pigment Color	Stability	Applications
(1) anthocyanin-saponite	Pigment is able to change color by manipulating pH level of the environment	pink/blue	Exhibited good stability against visible light and basic pH conditions	Atmospheric acidity sensor
(2) anthocyanin-saponite	Pigment is able to change color by manipulating pH level of the environment; pigment is observed to be environmentally friendly	pink/blue	Exhibited good stability against visible light and basic pH conditions	Atmospheric acidity sensor
(3) anthocyanin-saponite	Pigment is able to change color by manipulating pH level of the environment	light pink/light blue	Exhibited good pH stability	Color-changing advanced pigment
(4) anthocyanin-montmorillonite, anthocyanin-halloysite	Pigment is able to change color by manipulating pH level of the environment	dark brown/ light brown and pale red/light yellow, respectively.	Exhibited good thermal and chemical stability	pH indicators
(5) anthocyanin-montmorillonite	Higher concentrations of montmorillonite contribute to more stability.	red/dark red	Improved pH and color stability	Anthocyanin-based colorants
(6) anthocyanin-palygorskite	Pigment exhibited excellent acid/base allochronic behavior	bright pink/steel gray	Exhibited thermal and chemical corrosion resistance	Intelligent film that can detect the freshness of food
(7) anthocyanin-sepiolite	Hue, color, and stability of pigments are pH dependent	peach, orange, green, light purple, and yellow	Improved color and thermal stability	Fluorescent hybrid pigments

Table 2 shows a summary of the cited research, specifically on the characteristics of and stability of the pigments produced. It was observed that most of the pigments produced are affected by the pH level. The research cited showed that a color change occurs when the pH level is manipulated wherein the process was carried out by exposing the

hybrid pigment in an acidic atmosphere using hydrochloric acid (HCl) and then exposing it in a basic atmosphere using either ammonium hydroxide (NH4OH) or ammonia (NH3) for at least 6 to 10 minutes per exposure in a desiccator. Li et al. (2019) used slow oscillation at 70 revolutions per minute (rpm) for 24 hours at room temperature after applying the pigment into 10mL of hydrochloric acid and 10mL ammonium hydroxide, respectively. Silva et al. (2019) used sodium borate buffer solutions with a pH level of 10 and sodium acetate buffer solutions with pH levels of 4, 5, and 6 that were mixed with a sample of the pigments made and was stirred for 24 hours and was centrifuged and dried. This characteristic contributes to the overall stability of the pigment, particularly the chemical and pH stability of the produced pigment. It was also observed in the research done by Lima et al. (2020) that the pigments were environmentally friendly, making them a potentially useful pigment in terms of sustainability and safety. This is due to hybrid pigments possessing the carbon-based structures of natural pigments which are considered to be environmentally friendly as these do not generally include heavy metals or similar chemicals that are toxic and can cause damage to the environment but at the same time, possessing the stability and durability of inorganic materials (Bruni et al, 2019; Ebrahimi & Gashti, 2015; Li et al 2019). Ribeiro et al. (2020) mentioned that higher concentrations of montmorillonite contribute to more stability, which was observed throughout the experimentation.

The colors exhibited by the hybrid pigments made in each of the research varied across the research cited. It was observed in anthocyanin-saponite hybrid pigments produced in the research done by Lima et al. (2020a), Lima et al. (2020b), and Ogawa et al. (2017) that the colors exhibited by the hybrid pigment were pink or blue, although the pigment exhibited by Ogawa et al. (2017) was shown to exhibit lighter variants of the colors mentioned. The colors of the pigments are capable of changing from pink to blue depending on the pH level, wherein the hybrid pigment becomes pink when exposed to an acidic environment or blue when exposed to a basic environment. This principle also applies to the pigments produced by Li et al. (2019a) which exhibited dark brown or light brown colors for the anthocyanin-montmorillonite hybrid pigment and pale red or light-yellow colors for the anthocyanin-halloysite hybrid pigment; Ribeiro et al. (2018) which exhibited red or dark red colors for the anthocyanin-montmorillonite hybrid pigment and Li et al. (2019b) which exhibited bright pink or steel gray colors for the anthocyanin-palygorskite hybrid pigment. Lastly, the pigment produced by Silva et al. (2019) showed a variety of colors which included peach, orange, green, light purple, and yellow, as the pigments produced in this research were aimed to be bright and fluorescent, hence the large variety of colors. The differences in colors were mainly due to the different sources of anthocyanins used in each of the respective research cited.

All pigments have exhibited better stability in different aspects. The anthocyanin-saponite hybrid pigments by Lima et al. (2020a), Lima et al. (2020b), and Ogawa et al. (2017) have shown to be resistant to degradation due to pH changes in the environment as well as light. The anthocyanin-montmorillonite hybrid pigments by Li et al. (2019a) and Ribeiro et al. (2018) have shown improvements with thermal, chemical, light, pH, and color stability based on the cited research. The anthocyanin-halloysite hybrid pigment by Li et al. (2019a) has shown improved pH and color stability. The anthocyanin-palygorskite hybrid pigment by Li et al. (2019b) has shown stability against heat and chemical erosion. Lastly, the anthocyanin-sepiolite hybrid pigment by Silva et al. (2019) exhibited improved color and thermal stability. Each of the different improvements in stability was observed from the testing carried out in each of the research. The improvement in pH stability was noted due to the reversible behavior of pigments in terms of color-changing ability, wherein the pigments can change from one color to another and vice versa by exposing the pigment in an acidic or basic atmosphere. The improvement in light, thermal, and color stability was noted due to the decreased amount of fading or destruction under the light of the hybrid pigment. The increased stability is due to the inorganic component of the hybrid pigments, which were combined with the natural pigment through the methods mentioned. With the intercalations that occurred in the process, the mineral clays used were able to create another layer of protection which improved the overall stability of the hybrid pigment.

The pigments produced in the cited literature are shown to be useful in different applications. The saponite hybrid pigments are applicable as color-changing pigments as well as atmospheric acidity sensors. The montmorillonite hybrid pigments are useful as lake pigments, pH indicators, or colorants. The halloysite hybrid pigment is useful as a pH indicator. The palygorskite hybrid pigment was mentioned to be potentially useful in the development of an intelligent film that can detect the freshness of food. Lastly, the sepiolite hybrid pigment is useful as a fluorescent hybrid pigment. Based on the information, it was observed that most of the applications of the pigments are connected to the ability of the pigments to change color depending on the pH level, as the recommended applications were based on the mentioned observations.

3. CONCLUSIONS

This paper provides a systematic review of different research on hybrid pigments created with anthocyanins and several clay minerals. Hybrid pigments have been studied due to their environmentally friendly properties from natural pigments combined with the stability from synthetic pigments. Different research papers regarding hybrid pigments made with anthocyanins combined with different mineral clays, particularly saponite, montmorillonite, halloysite, palygorskite, and sepiolite, were discussed and elaborated. A comparison between the processes and interactions has shown that all the cited research utilized adsorption to combine the components, which led to the occurrence of intercalation between the anthocyanin and stabilizer, thus forming the hybrid pigment. It was observed that all the pigments, regardless of stabilizer used, exhibited color-changing properties, wherein the color of the pigment can be manipulated by changing the pH level of the environment. The pigments produced a variety of colors, which included pink, blue, red, brown, yellow, orange, purple, and several more colors. The stability of the pigments has improved, as described through each of the respective research cited, which included improvements in chemical stability, light stability, color stability, and thermal stability. With that in mind, the different possible applications of the hybrid pigments include acidity sensors, colorants, general-use lake pigments, and may also lead to the development of intelligent film capable of detecting the freshness of food. Overall, the paper has shown the development and improvement in hybrid pigment research, particularly with anthocyanin hybrid pigments.

4. ACKNOWLEDGMENTS

The researchers would like to acknowledge the following people: Dr. Francisco Franco, for guiding and helping the researchers as their research adviser; the researchers' parents for their unwavering support; Dr. Ethel Ong and Dr. Ofelia Rempillo for their guidance and support as the researchers' mentors; and the cited researchers who spent their time and effort producing the research used in this paper.

5. REFERENCES

Britannica, T. Editors of Encyclopaedia (2013). Adsorption. Encyclopedia Britannica. https://www.britannica.com/science/adsorption

Bruni, S., Cicala, N., Freschi, A., Longoni, M. (2019). Non-invasive identification of synthetic organic pigments in contemporary art paints by visible–excited spectrofluorimetry and visible reflectance spectroscopy. Spectrochimica Acta Part A: Molecular and Biomolecular Spectroscopy, 11, https://doi.org10.1016/j.saa.2019.117907

Dufosśe, L. (2014). Anthraquinones, the Dr Jekyll and Mr Hyde of the food pigment family. Food Research International, 65, 132-136. https://doi.org/10.1016/j.foodres.2014.09.012

Ebrahimi, I., & Parvinzadeh Gashti, M. (2016). Extraction of polyphenolic dyes from henna, pomegranate rind, and Pterocarya fraxinifolia for nylon 6 dyeing. Coloration Technology, 132(2), 162–176. https://doi:10.1111/cote.12204

Kasiri, M. & Safapour, S. (2014). Natural dyes and antimicrobials for green treatment of textiles. Environmental chemistry letters, 12(1), 1-13. https://doi.org/10.1007/s10311-013-0426-2

Lagaly, G., Ogawa, M., & Dékány, I. (2013). Clay mineral–organic interactions. In Developments in Clay Science (Vol. 5, pp. 435-505). Elsevier. https://doi.org/10.1016/B978-0-08-098258-8.00015-8

Li, S., Ding, J., Mu, B., Wang, X., Kang, Y., & Wang, A. (2019). Acid/base reversible allochroic anthocyanin/palygorskite hybrid pigments: Preparation, stability and potential applications. Dyes and Pigments, 171, 107738. https://doi:10.1016/j.dyepig.2019.107738

Li, S., Mu, B., Wang, X., Kang, Y., & Wang, A. (2019). A comparative study on color stability of anthocyanin hybrid pigments derived from 1D and 2D clay minerals. Materials, 12(20), 3287. https://doi.org/10.3390/ma12203287

Lima, L., Castro-Silva, F., Silva-Filho, E., Fonseca, M., & Jaber, M. (2020a). Saponite-anthocyanin pigments: Slipping between the sheets. Microporous and Mesoporous Materials, https://doi.org/10.1016/j.micromeso.2020.110148

Lima, L., Silva, F. Silva-Filho, E., Fonseca, M., Zhuang, G., & Jaber, M. (2020b). Saponite-anthocyanin derivatives: The role of organoclays in pigment photostability. Applied Clay Science, 191, https://doi.org/10.1016/j.clay.2020.105604

Ogawa, M., Takee, R., Okabe, Y., & Seki, Y. (2017). Bio-geo hybrid pigment; clay-anthocyanin complex which changes color depending on the atmosphere. Dyes and Pigments, 139, 561-565. https://doi.org/10.1016/j.dyepig.2016.12.054

Ribeiro, H. L., de Oliveira, A. V., de Brito, E. S., Ribeiro, P. R., & Azeredo, H. M. (2018). Stabilizing effect of montmorillonite on acerola juice anthocyanins. Food chemistry, 245, 966-973. https://doi.org/10.1016/j.foodchem.2017.11.076

Silva, G., da Silva, K., Silva C., Rodrigues, A., Oake, J., Gehlen, M., Bohne, C. & Quina, F.. (2019). Highly fluorescent hybrid pigments from anthocyanin-and red wine pyranoanthocyanin-analogs adsorbed on sepiolite clay. Photochemical & Photobiological Sciences, 18(7), 1750-1760. https://doi.org/10.1039/C9PP00141G

Silva, S., Costa, E., Calhau, C., Morais, R. , & Pintado, M. (2017). Anthocyanin extraction from plant tissues: A review. Critical reviews in food science and nutrition, 57(14), 3072-3083. https://doi.org/10.1080/10408398.2015.1087963

Singh, S., Gaikwad, K., & Lee, Y. (2018). Anthocyanin-A natural dye for smart food packaging systems. Korean Journal of Packaging Science & Technology, 24(3), 167-180. https://doi.org/10.20909/kopast.2018.24.3.167

Meta-Analysis on the Dissolution of Bamboo (*Bambusa*) Cellulose using NaOH/urea Aqueous Solution

Jasmin Nicole B. Cristobal, Joachim Xavier B. Po, Raissa Adellaide M. Sison, and Moira Justine R. Velina
De La Salle University Integrated School, Manila

Dr. Allan N. Soriano
Chemical Engineering Department, Gokongwei College of Engineering, De La Salle University, Manila

Abstract: Bamboo cellulose is a non-dangerous, biodegradable polymer with high elastic, compressive quality thereby beneficial in commercial and pharmaceutical industries. However, preparing it involves a complex procedure of solvent dissolution. NaOH/urea solution is a common solvent for cellulose dissolution, but its efficiency varies with temperature and concentration. Thus, this study aims to synthesize evidence on the efficiency of NaOH/urea solution in bamboo cellulose dissolution; identify the most suitable concentration and temperature of NaOH/urea; and determine the relationships between its concentration, temperature and bamboo cellulose' dissolution rate. Extracted data indicated the bamboo source sample, NaOH/urea concentration, temperature, and dissolution results from five databases and utilized Quality of Reporting of Meta-analyses (QUOROM) and Assessment of Multiple Systematic Reviews (AMSTAR) instruments for the studies' quality assessment. Among the studies, 93% utilized the concentration ratio of 7:12:81; therefore, concentration's minimal changes did not profoundly affect the dissolution, given the same temperatures. Out of fifteen studies, eight used -12°C affirming that minimal changes in temperature affect the dissolution results. The Chi-square test revealed that only temperature and concentration indicate a significant relationship ($x2=5.793$, $P<0.10$). The heterogeneity test displayed a small amount of heterogeneity ($I2= 33.42\%$, $P<0.10$; $I2= 1.8\%$, $P<0.10$) on the gathered data that may be clinically unimportant, making the data considerably homogeneous. Hence, this provides significant evidence validating the efficiency of 7:12:81 NaOH/urea aqueous solution at -12°C in the dissolution of bamboo cellulose.

Key Words: bamboo cellulose; bamboo cellulose dissolution; NaOH/urea; meta-analysis; heterogeneity test

1. INTRODUCTION

Bamboos are distinguished by woody and hollow culms, intricate rhizomes and branching processes, narrow leaf blades, and visible sheathing organs. One main component of bamboo is cellulose ($C6H12O6$), one of the most universal natural polymers on earth. It is a non-dangerous, biodegradable polymer with high elastic and compressive quality, but it has across the board use in different fields, like the pharmaceutical industry and the construction industry that incorporates cellulose insulation. However, the cellulose must be disintegrated first through solvation to melt it (Gupta et al., 2019).

Preparing bamboo cellulose is difficult and usually takes numerous steps, as there are many solvents to experiment with. Local cellulose must be dissolved in a solvent in order to melt it. Most of the dissolvable frameworks known have a restricted limit of disintegration that is poisonous and costly, restricting their mechanical capabilities. Another approach in cellulose dissolution shows that cellulose is soluble in aqueous NaOH underneath 268 K inside a particular focus scope of NaOH. This framework is modest, possibly non-contaminating, utilizes extremely regular synthetics, and is moderately simple to deal with (Alves, 2015). Therefore, the focal point of this study is to collect and analyze related studies about the dissolution of bamboo cellulose using NaOH/urea. Specifically, this work determines the most suitable concentration and temperature that can maximize the solubility of bamboo cellulose using NaOH/urea and the relationships between the concentration and temperature of NaOH/urea and the solubility of bamboo cellulose.

2. METHODOLOGY

In identifying the articles that were reviewed in this study, the researchers followed the created criterion while specifying certain "identifiers" from the paper and made use of a checklist set adapted from Porritt et al. (2014) in Table 1. The following set of keywords was used for searching: "Bamboo Cellulose," "Cellulose Dissolution," "Bamboo Cellulose Solvation," "Dissolution of Bamboo Cellulose," and "NaOH/urea." The bamboo sample sources were sorted into three categories, namely Bamboo Pulp, Bamboo Pulp Boards, and Pretreated Bamboo.

Table 1. *Criteria and identifiers for selection of studies (Porritt et al., 2014)*

Criteria	Details	Mark
Date	Any date of the study	✓
Language	Articles in the English, Filipino, or Chinese Language	✓
Peer-review	Only peer-reviewed studies	✓
Setting	Bamboo cellulose solvation done under given temperatures	✓
Methodology	Mixed-method research	✓
Publication	Only articles found in the following databases: Scopus, ScienceDirect, JSTOR, Directory of Open Access Journals (DOAJ), and ResearchGate	✓

This also utilized Quality of Reporting of Meta-analyses (QUOROM) (Russo, 2007) and Assessment of Multiple Systematic Reviews (AMSTAR) (Pizarro et al., 2021) instruments in assessing the quality of the studies from the database search. After the article screening process using Preferred Reporting Items for Systematic Reviews and Meta-Analyses (PRISMA) guidelines (Moher et al., 2009), as displayed in Figure 1, data will be extracted from the studies eligible for inclusion. These extracted data were presented in a tabular format that identified the NaOH/urea concentration, temperature, and dissolution rate from each study. Moreover, statistical analysis increased the reliability of findings through the heterogeneity chi-square test and Higgins' I^2 heterogeneity statistic, as these tests are also required in a meta-analysis. After conducting all statistical treatments, these results were used in further analysis in determining the most suitable concentration and temperature for bamboo cellulose's maximized solubility in NaOH/urea aqueous solution.

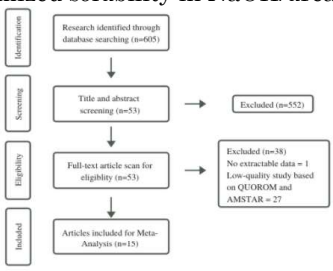

Figure 1. *Adapted PRISMA article screening process (Moher et al., 2009)*

3. RESULTS AND DISCUSSION

In gathering studies, a total of 605 studies were available from the databases that were searched using the keywords. From these studies, 53 studies chosen based on the title were screened and underwent the identification of studies wherein screening of the abstract and full text was executed. Of these, only 15 studies have met the criteria of quality assessment and were used for data extraction, as shown in the screening process in Figure 1.

Furthermore, the study of Yang et al. (2018) used bamboo pulp boards obtained from Guizhou, China which were dissolved with 7% NaOH/12% urea/81% distilled water at -12 °C. It was found that as soon as cellulose fibers are placed into NaOH/urea aqueous solution, they swell, and part of the intra- and intermolecular hydrogen bonding are destroyed. The work of Chen et al. (2015) used bamboo pulps which were obtained after delignification with sodium chlorite and alkaline treatment with 25% potassium hydroxide from bamboo. It was dissolved in a 7/12 wt % NaOH/urea solution at -12.6 °C. In this study, bamboo pulps just swelled in the NaOH/urea aqueous solution since it had been demonstrated that only cellulose with a viscosity-average molecular weight below 10.0×10^4 Da could be completely dissolved in NaOH/urea aqueous solution. Shi et al. (2017) used commercial bamboo dissolving pulp boards provided by Sichuan Lee & Man., while commercial bamboo dissolving pulp boards provided by Sichuan Liwen Paper Co. Ltd. were also used by Shi et al. (2017). Both were dissolved with 7% NaOH and 12% urea aqueous solution at -13 °C, with a dissolution rate of 43.4.

Additionally, Lin et al. (2017) used bamboo pulp obtained from Sichuan, China, and dissolved it in 7% NaOH, 12% urea, and 81% H2Osolution at -13 °C. After stirring for 10 min, they observed a homogenous cellulose solution. Moreover, bamboo (Phyllostachys heterocyla) pulp from Guizhou Chitanhua Paper Industry Co., Ltd. was used by Zhu et al. (2015), which was dissolved at 7% NaOH and 12% urea, precooled to 4 °C and maintained at -12 °C. It had a dissolution rate of 100% with a transparent and viscous bamboo pulp cellulose solution. Similar results were observed by Nguyen et al. (2019) where they used micron-size White Bamboo (Dendrocalamus membranaceus Munro) fibrils, a pretreated bamboo from Hoa Binh Province, Vietnam, which was dissolved in 7% NaOH, 12% urea, and 81% distilled water at 5°C. Their results show almost 24% dissolution with a semi-transparent to transparent cellulose. In the study of Tang et al. (2017), cellulose was obtained from a bamboo dissolving pulp board from Sichuan, China, where it was dissolved in NaOH/urea/water solution (7:12:81 by weight) at -12°C. In the cellulose I crystals, the hydrogen bonds were destroyed when the cellulose I crystals were dissolved in NaOH/urea solution.

Moreover, Li et al. (2011) also used pretreated bamboo, but with partially delignified bamboo (Neosinocalamus affinis) culms which were 100% dissolved with 7% sodium hydroxide/12% urea solution at -12 °C. Figure 2 summarizes the dissolution rate of the aforementioned individual studies while Table 2 summarizes the data extracted from these studies.

Out of the 15 studies, 14 studies (93%) utilized the 7:12:81 ratio for the concentration of NaOH/urea aqueous solution (see Figure 3). Almost all of these studies showed the said concentration to be 100% effective for bamboo cellulose dissolution. Varying dissolution rate may have resulted from other factors like vigorous stirring (Nguyen et al., 2019), ultrasound/ethanol pretreatment (Li et al., 2021), and vacuum oven drying (Shi et al., 2017 & Shi et al., 2017); yet, they are still proven to be effective. However, the study of Ma et al. (2017) used the concentration ratio of 7.5:11:81.5. The minimal change in the concentration did not greatly affect the dissolution of bamboo cellulose, given that the temperature is the same. For these reasons, the optimum NaOH-urea-distilled water ratio for dissolving bamboo cellulose is 7:12:81.

Table 2. *Summary of the data extracted*

Bamboo Source Sample	NaOH-urea-distilled water Concentration	Temperature	Dissolution Rate	Author/s	Year
Bamboo Pulp	7:12:81	-12.5 °C	100%	Li et al.	2015
Bamboo Pulp	7.5:11:81.5	-7 °C	100%	Zhai et al.	2018
Pretreated Bamboo	7:12:81	-12 °C	61%	Kong et al.	2021
Bamboo Pulp	7:12:81	-12 °C	75.1 -77.7%	Li et al.	2010
Bamboo Pulp	7:12:81	-12 °C	83.6% - 86.6%	Li et al.	2021
Bamboo Pulp Boards	7:12:81	-12 °C	61%	Yang et al.	2018
Bamboo Pulp	7:12:81	-12.6 °C	0%	Chen et al.	2015
Bamboo Pulp Boards	7:12:81	-13 °C	43.4%	Shi et al.	2017
Bamboo Pulp Boards	7:12:81	-13 °C	43.4%	Shi et al.	2017
Bamboo Pulp	7:12:81	-13 °C	100%	Lin et al.	2017
Bamboo pulp	7:12:81	-12 °C	100%	Zhu et al.	2015
Pretreated Bamboo	7:12:81	5 °C	24%	Nguyen et al.	2019
Pretreated Bamboo	7:12:81	-12 °C	100%	Lou et al.	2015
Bamboo Pulp Board	7:12:81	-12 °C	100%	Tang et al.	2017
Pretreated Bamboo	7:12:81	−12°C	100%	Li et al.	2011
Bamboo pulp	7:12:81	-12 °C	100%	Zhu et al.	2015
Pretreated Bamboo	7:12:81	5 °C	24%	Nguyen et al.	2019
Pretreated Bamboo	7:12:81	-12 °C	100%	Lou et al.	2015
Bamboo Pulp Board	7:12:81	-12 °C	100%	Tang et al.	2017
Pretreated Bamboo	7:12:81	−12°C	100%	Li et al.	2011

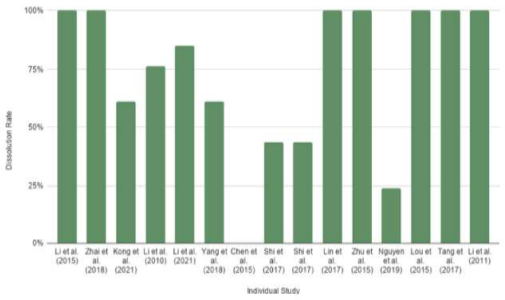

Figure 2. *Pooled dissolution percentages of individual studies*

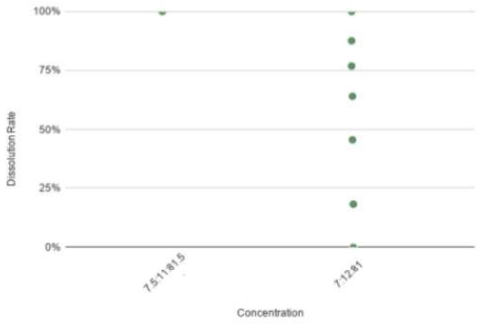

Figure 3. *Effect of concentration of the solution on dissolution rate of bamboo cellulose*

Meanwhile, 8 out of 15 studies dissolved bamboo cellulose at a relatively lower temperature, specifically at -12°C. Nearly all of the studies show that bamboo cellulose can be 100% dissolved using NaOH/urea at -12°C, as shown in Figure 4. Results obtained by Li. et al. (2011) and Zhu et al. (2015) present that the most effective and efficient way to completely dissolve pretreated bamboo and bamboo pulp was at -12°C. On the other hand, Nguyen et al. (2019) and Chen et al. (2015) dissolved cellulose at 5°C and -12.6°C. Minimal change in the temperature affected the dissolution results since at -12.6°C, the bamboo pulp just swelled in the NaOH/urea aqueous solution, and 0% of the pulp was dissolved. Moreover, Zhai et al. (2018) argued against the application of temperature above 0°C in the solution as cellulose would not be dissolved in that case as the swelling, softening, and dissolving exothermic processes can only protect the pulp fibers at low temperatures below that degree. Under these conditions, the most ideal temperature for the solvation of bamboo cellulose is at -12°C.

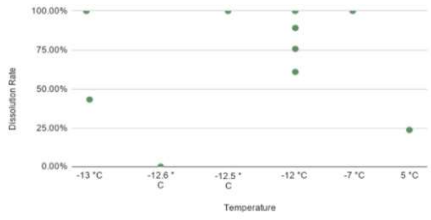

Figure 4. *Effect of solution's temperature on dissolution rate of bamboo cellulose*

To solidify the findings, statistical analyses were done. Chi-square test was used to confirm if there were significant relationships between variables. Upon analysis, bamboo sample sources and temperature of the aqueous solution ($x2=3.945$, $P<0.10$) were independent of each other. Concentration of aqueous solution and bamboo sample sources ($x2=1.587$, $P<0.10$) also have no significant relationship. Conversely, temperature and concentration ($x2=5.793$, $P<0.10$) of the aqueous solution indicates relation. Furthermore, determining statistical heterogeneity is important for a meta-analysis to detect variability among factors influencing the intervention. In this analysis, a p-value of 0.10 was used to determine statistical significance as nonsignificant results were not considered evidence for heterogeneity. The Higgins' I2 test revealed a small amount of heterogeneity on the gathered data that may be clinically unimportant, thereby making the data considerably homogeneous: ($I2= 33.42\%$, $P<0.10$ for source and temperature; $I2= 1.8\%$, $P<0.10$ for source and concentration). Visual assessment of the plotted rates in Figure 4 showed that four studies (Lin et al., 2017; Shi et al., 2017; Chen et al., 2015; Nguyen et al., 2019) accounted for the heterogeneity with extreme temperatures as the possible reason ($I2= 69.52\%$, $P<0.10$). Hence, the substantial evidence corroborates the guaranteed efficiency of NaOH/urea aqueous solution at low temperature in the dissolution of bamboo cellulose.

4. CONCLUSIONS

Accounting for 93% of all studies, the 7:12:81 ratio for the concentration of NaOH/urea aqueous solution dominated the data and mostly exhibited a 100% efficiency for the dissolution of bamboo cellulose. Therefore, the optimum NaOH-urea-distilled water ratio for dissolving bamboo cellulose is 7:12:81. Meanwhile, 8 out of 15 studies dissolved bamboo cellulose at a relatively lower temperature, specifically at -12 °C. Minimal change in the temperature affected the dissolution results with temperatures exceeding 0 °C labeled as protection-inefficient and receding -12 °C resulted in swelling; thus, the most ideal temperature for the solvation of bamboo cellulose is at -12 °C. The Chi-square test showed that both the relationship of bamboo sample sources and temperature of the aqueous solution and the relationship of concentration of aqueous solution and bamboo sample sources have no significant relationship. Meanwhile, temperature and concentration indicate relation. The test for heterogeneity displayed a small amount of heterogeneity on the gathered data that may be clinically unimportant thereby making the data considerably homogeneous. The heterogeneity of the data ($I2= 69.52\%$, $P<0.10$) was mainly affected by the extreme temperatures used by the individual studies. Overall, the significant evidence validates the efficiency of NaOH/urea aqueous solution at low temperature in the dissolution of bamboo cellulose.

5. ACKNOWLEDGMENTS

Before all else, praises to De La Salle University - Senior High School for providing us an avenue to explore our passions and enabling us to unlock our innate research talents. We would like to thank our families for their undying support and guidance in our everyday life, especially in the making of this research project. They have provided us with everything we need in preparation for this study: funding, patience, and understanding. To our friends who were always there when we needed help, thank you for being the shoulders we could lean on. We are sincerely grateful for all the help you all have given to us, may it be academically and mentally wise.

Above all, the researchers share their deepest gratitude to their Research Adviser, Dr. Allan Soriano, for guiding and supervising them. It was a privilege to work under his wing, and the researchers are grateful for what he has offered them. The researchers' completion of this study could not have been successful without his support. It is with no doubt the researchers believe the lifelong learnings he has instilled will carry on beyond research consultations.

6. REFERENCES

Alves, L. H. (2015). Cellulose solutions: dissolution, regeneration, solution structure and molecular interactions. Coimbra, Portugal: Universidad de Coimbra. DOI: 10.5772/61402

Chen, J., Guan, Y., Wang, K., Zhang, X., Xu, F., & Sun, R. (2015). Combined effects of raw materials and solvent systems on the preparation and properties of regenerated cellulose fibers. Carbohydrate Polymers, 1(128), 147–153. https://doi.org/10.1016/j.carbpol.2015.04.027

Gupta, P., Raghunath, S., Prasanna, D., Venkat, P., Shree, V., Chithananthan, C., . . . Geetha, K. (2019, May 13). An update on overview of cellulose, its structure and applications. In A. Pascual & M. Martín (Eds) Cellulose. IntechOpen. DOI: 10.5772/intechopen.84727

Kong, W., Yu, G., Xing, J., Kong, R., Liu, M., & Shi, Y. (2021). Effect of the Dissolving Method on the Dissolution of Dissolving Pulp Cellulose Fibers with Different Dried-States in Different NaOH/additives Aqueous Solutions DOI: 10.21203/rs.3.rs-167392/v1

Li, M-F., Fan, Y-M., Xu, F., & Sun, R-C. (2011). Structure and thermal stability of polysaccharide fractions extracted from the ultrasonic irradiated

and cold alkali pretreated bamboo. Journal of Applied Polymer Science. https://doi.org/10.1002/app.33491

Li, M.-F., Fan, Y.-M., Xu, F., Sun, R.-C., & Zhang, X.-L. (2010). Cold sodium hydroxide/urea-based pretreatment of bamboo for bioethanol production: Characterization of the cellulose rich fraction. Industrial Crops and Products, 32(3), 551–559. https://doi.org/10.1016/j.indcrop.2010.07.004

Li, M.-F., Yong-Ming Fan, Feng Xu, & Sun, R.-C. (2021). Characterization of Extracted Lignin of Bamboo (Neosinocalamus Affinis) Pretreated with Sodium Hydroxide/Urea Solution at Low Temperature. BioResources, 5(3), 1762–1778. https://ojs.cnr.ncsu.edu/index.php/BioRes/article/view/BioRes_05_3_1762-1788_Char_Extracted_Lignin_Bamboo

Li, R., Wang, S., Lu, A., & Zhang, L (2015). Dissolution of cellulose from different sources in an NaOH/urea aqueous system at low temperature. Cellulose, 22(1), 339–349. DOI:10.1007/s10570-014-0542-6

Lin, X., Ma, W., Wu, H., Huang, L., Chen, L., & Takahara, A. (2017). Fabrication of cellulose based superhydrophobic microspheres for the production of magnetically actuatable smart liquid marbles. Journal of Bioresources and Bioproducts, 2(3), 110-115. DOI: 10.21967/jbb.v2i3.132

Lou, H., Zhu, D., Yuan, L., Lin, H., Lin, X., & Qiu, X. (2015). Fabrication and property of low crystallinity nanofibrillar cellulose and nanofibrillar cellulose graphene oxide composite. The Royal Society of Chemistry, 5(83), 67568-67573. https://doi.org/10.1039/C5RA13181B

Moher, D., Liberati, A., Tetzlaff, J., Altman, D.G., The PRISMA Group (2009). Preferred Reporting Items for Systematic Reviews and Meta-Analyses: The PRISMA Statement. Open Med 2009, 3(3), 123-130. http://dx.doi.org/10.1016/j.ijsu.2010.02.007

Nguyen, D. D., Vu, C. M., Vu, H. T., & Choi, H. J. (2019). Micron-Size White Bamboo Fibril-Based Silane Cellulose Aerogel: Fabrication and Oil Absorbent Characteristics. Materials, 12(9), 1407. https://doi.org/10.3390/ma12091407

Pizarro, A.B., Carvajal, S., Buitrago-López, A .(2021). Assessing the methodological quality of systematic reviews using the AMSTAR tool. Colombian Journal of Anesthesiology. 49(1), 913. : https://doi.org/10.5554/22562087.e913

Porritt, K., Gomersall, J., & Lockwood, C. (2014). JBI's Systematic Reviews: Study selection and critical appraisal. AJN, American Journal of Nursing, 114(6), 47–52. https://doi.org/10.1097/01.naj.0000450430.97383.64

Russo M. W. (2007). How to Review a Meta-analysis. Gastroenterology & hepatology, 3(8), 637–642.https://www.ncbi.nlm.nih.gov/pmc/articles/PMC3099299/#:~:text=Meta%2Danalysis%20is%20a%20systematic,a%20treatment%20intervention%20or%20exposure.

Shi, Y., Zhang, K., Sun, H., Zhu, Y., Hu, Z., Zheng, Q., & Yang, F. (2017). Dissolution behavior of higher DP bamboo dissolving pulp fiber in NaOH/ additive aqueous solution. Functional Materials, 48(6), 6080-6085. https://doi.org/10.3969/j.issn.1001-9731.2017.06.014

Shi, Y., Zhang, K., Ya-tong, Z., Zhen-xing, H., Nan, S., Miai-li, B., & Lin, P. (2017). The Influence of Alkali Pretreatment on the Dissolution of Bamboo Dissolving Pulp in NaOH/Urea System. Chinese Journal of Paper Industry, 32(2), 12–16. Transactions of China Pulp and Paper. https://doi.org/10.11981/j.issn.1000-6842.2017.02.12

Tang, Z., Li, W., Lin, X., Xiao, H., Miao, Q., Huang, L., Chen, L., & Wu, H. (2017). TEMPO-Oxidized Cellulose with High Degree of Oxidation. Polymers, 9(12), 421. https://doi.org/10.3390/polym9090421

Yang, X., Fei, B., Ma, J., Liu, X., Yang, S., Tian, G., & Jiang, Z. (2018). Porous nanoplatelets wrapped carbon aerogels by pyrolysis of regenerated bamboo cellulose aerogels as supercapacitor electrode. Carbohydrate Polymers, 180, 385–392. https://doi.org/10.1016/j.carbpol.2017.10.013

Zhai, R., Ma, J., Hu, Z., & Hou, J. (2018). The Effects of NaOH-Urea Aqueous Solution on the Strength and Softness Properties of Bamboo Ligno-cellulosic Fibers. BioResources, 13(1), 1088-1106. https://doi.org/10.15376/biores.13.1.1088-1106

Zhu, H., Zhang, Y., Yang, X., Liu, H., Zhang, X., & Yao, J. (2015). An Eco-friendly One-Step Synthesis of Dicarboxyl Cellulose for Potential Application in Flocculation. Industrial & Engineering Chemistry Research, 54(10), 2825–2829. https://doi.org/10.1021/ie503020n

Development of Generalized Correlation for Electrical Conductivity Prediction of Pure Ionic Liquid

Carlos Gabriel A. Arguelles, Carlos John B. Dionio,
John Matthew C. Enciso, Ar Jettherson T. Go, and Paul Andrei M. Jardiolin
De La Salle University Integrated School, Manila

Dr. Allan N. Soriano
Chemical Engineering Department, Gokongwei College of Engineering,
De La Salle University, Manila

Abstract: Ionic liquids are salts in liquid form that are composed of short-lived ion pairs. They are the new trend of solvent because of their very low vapor pressure, good chemical and thermal stability, and melting temperatures lower than 100°C. Pure ionic liquids contain ions that can conduct electricity or serve as electrolytes. But experimentation using ionic liquids would be expensive. This study aims to develop a generalized correlation for the electrical conductivity prediction of pure ionic liquids. The researchers gathered data of pure ionic liquids that involved the electrical conductivity property from the ThermoIL Database. The collected data were then trimmed based on a developed scheme and classifications. After trimming the data, the researchers evaluated the data using MATLAB software. The residual value was calculated, and a parity plot was constructed to test the models' accuracy. The researchers gathered 2,425 data points from 310 references and were trimmed to 220 data points from 21 references. The parity plot and graph of the residuals plotted against pressure showed that the experimental and calculated values were close. Results showed that the electrical conductivity of pure ionic liquids could be predicted using a model patterned to Pitzer correlation with reduced temperature and reduced pressure as variables. Data with two or more references and low uncertainty made a good result on the models to create a generalized correlation via curve fitting.

Key Words: pure ionic liquids; electrical conductivity; generalized correlation; data trimming; data mining

1. INTRODUCTION

Ionic liquids (ILs) are liquid salts that are composed of ions and short-lived ion pairs. ILs are potential substitutes for dangerous solvents for preparing solutions such as gels, composites, and polymeric belts (Shakeel et al., 2019). Some of the interesting properties of ILs include Chemical and thermal stability, very low vapor pressures, and melting temperatures below 100°C. In 1914, Paul Walden was the first to find ILs. Walden was looking for liquid molten salts at a specific temperature to use in his equipment without fulfilling any specifications. The melting point of ethylammonium nitrate (EtNH3NO3), the first IL found, is 12°C, according to Walden (Welton, 2018). ILs are also environmentally friendly, easily recyclable, highly efficient, and similarly structured to conventional solvents. As a result, these liquids have become the latest solvent standard.

The electrical conductivity of ILs is also an intriguing property. Electrical conductivity (σ), also known as conductance, is the potential of a material to bear an electric current (Helmenstine, 2020). Based on the temperature, each liquid material has a different conductance. Electrical conductivity increases by two to three percent with every one-degree Celsius increase in temperature. Between liquid substances, pure water has the lowest conductivity. That is primarily due to the low number of ions present in pure water. ILs, in contrast, have many ions that are essential in conductance. An aqueous substance's conductivity increases as the number of ions present increases, indicating a solid electrolyte. Thus, ILs are used in commercial devices as an electrolyte with longer battery life because of their low vapor pressure.

Conducting experiments or research utilizing ionic liquids would be expensive. One of the cheapest IL in the market is the Trihexyltetradecylphosphonium bis(2,4,4-trimethylpentyl) phosphinate, which costs $21 (approximately Php 1066.50) for five grams. This is

the main reason why most researchers do data mining rather than doing experiments. Data collected by experimental procedures of previous researchers are collected and compiled on a database accessed on the internet. These data, however, are not being utilized well. Data mining is the process of discovering correlations, patterns, and trends using pattern recognition technologies and statistical and mathematical techniques (Gartner Group, 2014). This process is an efficient way to utilize available data on the internet. There are different data mining methods, and each has different uses depending on the situation, which can help businesses and researchers (Loginworks Software, 2014).

This research aims to develop a generalized correlation for the prediction of the electrical conductivity of pure ionic liquids. It also seeks to determine the most suitable data available from literature (ThermoIL Database) using the data trimming process and create the generalized correlation via-curve fitting the data using the MATLAB Software. This study, on the other hand, will help other researchers develop their research, especially those who have similar topics to this study. Furthermore, manufacturers can also innovate new products and find an ionic liquid that can serve as an electrolyte and improve its quality using this mathematical model.

This study solely aims to create a correlational model that can help predict the electrical conductivity of pure ILs. It does not cover the uses of knowing the electrical conductivity of ILs; it will only serve as a stepping stone to other researchers that plan to create commercial applications from pure ILs. This study will also gather data from the ThermoIL database only. The researchers will be cross-referencing, and they will use the data to create a correlational model for predicting pure IL's electrical conductivity. The study will not perform any laboratory experiments to justify the claims. The study will not include binary mixtures and tertiary mixtures, and ILs that do not have standard pressure.

2. METHODOLOGY

2.1 Collection of Data from ThermoIL database

The researchers first collected data. These data were collected from the ThermoIL database, covered pure ionic liquids, and focused on an ionic liquid's electrical conductivity property. The researchers also gathered the chemical structures for each of the chemical formulas for its visual representation. Each IL was given codes according to their cation and anion. The researchers obtained the International Union of Pure and Applied Chemistry (IUPAC) name of the pure IL, molar weight in terms of grams per mole (g/mol), pressure in terms of kilopascal (kPa), the temperature range in terms of Kelvin (K), electrical conductivity range in terms of siemens per meter (S/m), and its reference.

2.2 Data Trimming

The researchers gathered data of pure ILs reporting electrical conductivity from all available literature in the ThermoIL database. All of the data gathered from experimental procedures have been assessed carefully to ensure only accurate and reliable data will be collected and used since this research will only conduct computational methods. Figure 1 shows a developed scheme for the data trimming process and was classified into three categories as follows; (i) systems with more than two available references, (ii) systems with two available references, and (iii) systems with only one reference. Different data trimming procedures were done in each category. The data from the systems with more than two references had been trimmed by only using the most consistent data with the other references. For systems with two references, the most accurate between them was chosen based on the uncertainty reported. Systems with only one reference had been considered automatically; however, systems that only have two or fewer data points were removed and were not considered. Trimmed data were then investigated to gather the cations and anions (Soriano, Agapito, Lagumbay, Caparanga & Li, 2010).

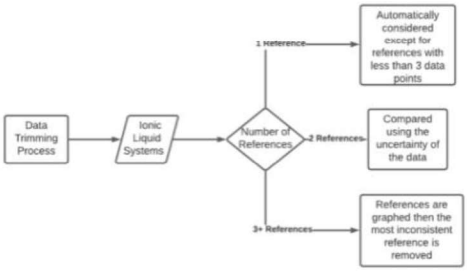

Figure 1. *Data trimming flowchart*

2.3 Development of Generalized Correlation for Electrical Conductivity

The researchers created a mathematical model. It was used to predict the electrical conductivity of a pure ionic liquid. The model used is patterned to the general Pitzer correlation to fit electrical conductivity, σ, as a function of temperature, T. It is represented as:

= T0+ T1 (Eq. 1) where ω is the acentric factor for the ionic liquid. For this study, the parameters T0 and T1

were defined as quadratic functions of the temperature:

To=A1+ A2TTc+ A3TTc2
(Eq. 2)

T1=A4+ A5TTc+ A6TTc2
(Eq. 3)

The ratio of T and Tc is the reduced temperature, where Tc is the critical temperature of the ionic liquid. Empirical constants were represented as An (n = 1 to 6), and acentric factors and critical data were obtained from the paper of Valderrama, Forero, and Rojas (2012). Pitzer's equations are used to describe the activity coefficients of aqueous electrolytes.

2.4 Testing of Model

The researchers tested the model's accuracy by finding the distance between the experimental (literature) data and calculated (predicted) data. It was determined using the Residual as follows:

Residual = y - y

(Eq. 4) where y is the experimental electrical conductivity and y is the calculated electrical conductivity.

The researchers also created a parity plot, a plot used to compare experimental or literature values to the calculated or tabulated values. Its purpose is to determine whether the obtained values are acceptable or not.

3. RESULTS AND DISCUSSION

The researchers were able to collect the data needed in this research from the ThermoIL database. They have collected 2,425 data points from 310 reference studies, which observed the criteria required. The gathered electrical conductivity of pure ILs from the database were all under standard pressure and are in the liquid phase.

The data collected underwent a data trimming process to remove unnecessary and insignificant data. ILs were grouped for data trimming according to the number of references available. References with less than three data points were first removed from all the groups of ILs. The data with only one reference was retained, while for those with two references, the data with high uncertainty were removed. The data with more than two references were plotted in a graph. The data that do not fit the dataset was then removed. Figure 2 shows an example of a graph used in the data trimming process for ILs with more than two references. The reference that contains the yellow points was removed from the dataset.

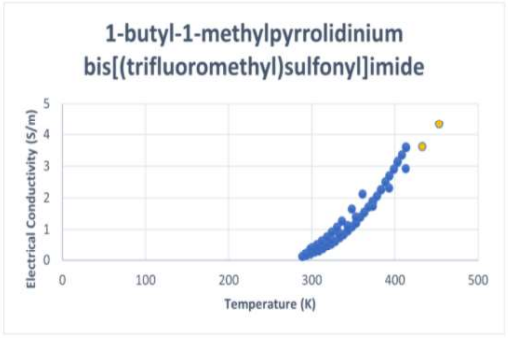

Figure 2. *Example of data trimming for ILs with more than two references*

The data trimming process reduced the number of data points and references to 2,231 and 203, respectively. Due to data unavailability, the numbers were cut off again after the researchers gathered the acentric factors and critical constants needed for the process. ILs with incomplete factors and constants were removed, decreasing the number of data points and references to 220 and 21, respectively. Table 1 shows the summary of the trimmed data used to develop the generalized correlation.

In using MATLAB software, equations 2 and 3 were manipulated to reduce the deviation of the experimental data and calculated data. Equations 5 and 6 show the new equations used in the process with the addition of pressure and critical pressure values. Figure 3 shows the parity plot that displays the relationship between the experimental and calculated data. It shows that most of the data points are near the line of equality, indicating that most of the calculations are close to experimental values.

$$T^{o} = A_1 + A_2\left(\frac{T}{T_c}\right) + A_3\left(\frac{T}{T_c}\right)^2 + A_4\left(\frac{P}{P_c}\right) + A_5\left(\frac{P}{P_c}\right)^2 \quad \text{(Eq. 5)}$$

$$T^{1} = A_6 + A_7\left(\frac{T}{T_c}\right) + A_8\left(\frac{T}{T_c}\right)^2 + A_9\left(\frac{P}{P_c}\right) + A_{10}\left(\frac{P}{P_c}\right)^2 \quad \text{(Eq. 6)}$$

Table 1. Summary of the trimmed data used in the development of the generalized correlation

IUPAC Name	MW	Acentric Factor	Critical Temp.	Critical Pressure	Pressure	Temp. Range	Electrical Conductivity Range	Data Points	Reference
1-(2-hydroxyethyl)-3-methylimidazolium bis[(trifluoromethyl)sulfonyl]imide	407.3	0.5172	1297.5	3307	101.325	283.15 - 353.15	0.1319 - 1.815	15	Liu et al. (2015)
1,2-dimethyl-3-propylimidazolium bis[(trifluoromethyl)sulfonyl]imide	419.36	0.32	1269.7	2746	100	293.15-323.15	0.196 - 0.687	7	Papovic et al. (2016)
1-butyl-3-methylimidazolium tetrafluoroborate	226.03	0.8877	843.2	2038	101.325	303 - 353	0.416 - 2.144	11	Iwasaki et al. (2017)

1-butyl-3-methylimidazolium tetrafluoroborate	226.03	0.8877	643.2	2038	101.325	298.15-333.15	0.36 - 1.516	8	Pandit et al. (2016)
1-butyl-3-methylimidazolium thiocyanate	197.30	0.4781	1047.4	1938	101.325	298.15-333.15	0.644 - 1.862	8	Pandit et al. (2016)
1-butyl-3-methylimidazolium tricyanomethane	229.29	0.9266	1185.1	2114	101.325	293.25 - 379.25	1.027 - 4.56	11	Zubeir et al. (2015)
1-butylpyridinium bis(trifluoromethyl)sulfonyl]imide	416.35	0.2505	1229.1	2771	101.325	293-344	0.191 - 0.937	6	Dzida et al. (2019)
1-butylpyridinium bis(trifluoromethyl)sulfonyl]imide	416.35	0.2505	1229.1	2771	101.325	278.15 - 438.15	0.1186 - 5.243	15	Nazet et al. (2017)
1-ethyl-2,3-dimethylimidazolium bis(trifluoromethyl)sulfonyl]imide	405.33	0.2794	1258.9	2975	100	293.15-323.15	0.309 - 0.92	7	Papovic et al. (2016)
1-ethyl-3-methylimidazolium acetate	170.21	0.5889	807.1	2919	101	288.15 - 353.15	0.151 - 2.223	14	Zhang et al. (2017)
1-ethyl-3-methylimidazolium acetate	170.21	0.5889	807.1	2919	101	298.15 - 418.15	0.2776 - 6.917	13	Nazet et al. (2015)
1-ethyl-3-methylimidazolium acetate	170.21	0.5889	807.1	2919	101	298.15 - 323.15	0.2875 - 0.918	6	Oliveira et al. (2015)
1-ethyl-3-methylimidazolium methanesulfonate	206.26	0.3307	1026	4813	101.325	273.15 - 353.15	0.04134 - 1.994	19	Harris et al. (2016)
1-ethyl-3-methylimidazolium trifluoromethanesulfonate	260.23	0.3255	992.30	3584	101.325	273.15 - 353.15	0.346 - 3.287	13	Harris et al. (2016)
1-ethyl-3-methylimidazolium trifluoromethanesulfonate	260.23	0.3255	992.30	3584	101.325	297.65-304.65	0.81 - 1.14	5	Aranowski et al. (2016)
1-ethyl-3-methylimidazolium trifluoromethanesulfonate	260.23	0.3255	992.30	3584	101	288.15 - 333.15	0.605 - 2.236	3	Asenbauer et al. (2017)
1-ethylpyridinium bis[(trifluoromethyl)sulfonyl]imide	388.3	0.1671	1207.9	3275	101.325	303-343	0.528 - 1.335	5	Dzida et al. (2019)
1-octyl-3-methylimidazolium bis[(trifluoromethyl)sulfonyl]imide	475.47	0.4811	1317.8	2098	101	273.15 - 468.15	0.0308 - 4.029	29	Nazet et al. (2015)
1-octyl-3-methylimidazolium bis[(trifluoromethyl)sulfonyl]imide	475.47	0.4811	1317.8	2098	100	293.15 - 323.15	0.106 - 0.361	7	Papovic et al. (2016)
butylammonium formate	119.16	0.5182	521.1	3466	100	293.15 - 333.15	0.287 - 0.873	9	Wei et al. (2018)
propylammonium formate	105.14	0.4839	496.6	3919	101.325	293.15 - 333.15	0.31 - 1	9	Chhotaray et al. (2015)

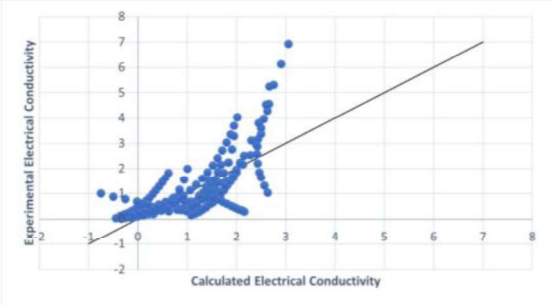

Figure 3. *Parity plot*

The residual, on the other hand, is shown in figures 4 and 5, plotted against the reduced pressure (Pr) and reduced temperature (Tr), respectively. Both figures show the patterned mathematical model is appropriate for the dataset. In addition, the plot shows that the residuals are not far from zero, indicating that the calculated electrical conductivity is close to the experimental electrical conductivity. It also shows that the model has both underprediction and overprediction of the data.

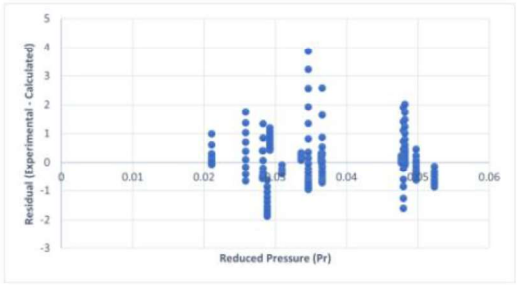

Figure 4. *Residual plotted against reduced pressure*

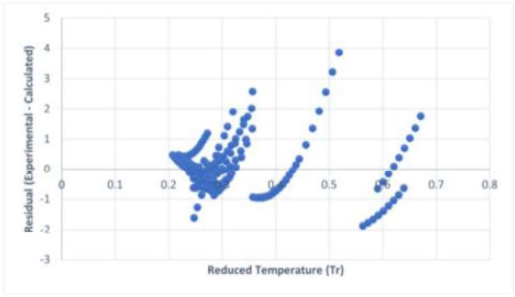

Figure 5. *Residual plotted against reduced temperature*

According to Van der Waals' Corresponding States Principle, substances behave alike at the same reduced states. Figure 6 shows the relationship between reduced pressure and the experimental data. Different colored lines connect the substances with the same reduced temperature. The graph for each reduced temperature follows the same pattern. However, as the reduced temperature decreases, the graph will have an inconsistent pattern compared to the graphs in Figure 6 and more complicated as shown on the graph of Tr = 0.26.

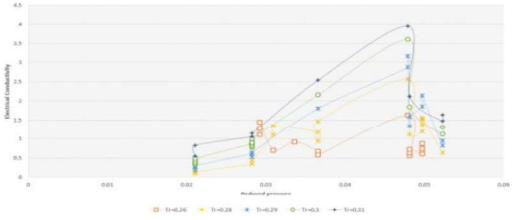

Figure 6. *Reduced pressure plotted against electrical conductivity*

4. CONCLUSIONS

The researchers have successfully created a model that can predict the electrical conductivity of pure ionic liquids. Using data trimming, the researchers have identified the most suitable data to be used in the study. Still, the unavailability of constants needed for the process significantly affected the number of the data point used in the study. Most of the calculated data from the model are close to their respective experimental values. However, there are some systems that the researchers have underestimated. Thus, further research should be conducted to have a more accurate prediction of the property. The model produced by this study can be used as a reference model for future studies that will be conducted. Manufacturers that would use this model as a basis for their research and innovation of their products should note some Ionic Liquid system that has been underestimated to be avoided since it is not accurate enough compared to other systems.

5. ACKNOWLEDGMENTS

The researchers would like to express their deepest gratitude to their marvelous adviser, Dr. Allan N. Soriano, for his guidance in accomplishing this research. His consideration and patience with his research mentees were greatly appreciated.

6. REFERENCES

Aranowski, R., Cichowska-Kopczyńska, I., Dębski, B., & Jasiński, P. (2016). Conductivity and viscosity changes of imidazolium ionic liquids induced by H2o and Co2. Journal of Molecular Liquids, 221, 541-546.

Asenbauer, J., Hassen, N. B., McCloskey, B. D., & Prausnitz, J. M. (2017). Solubilities and ionic conductivities of ionic liquids containing lithium salts. Electrochimica Acta, 247, 1038-1043.

Chhotaray, P. K., & Gardas, R. L. (2015). Structural dependence of protic ionic liquids on surface, optical, and transport properties. Journal of Chemical & Engineering Data, 60(6), 1868-1877.

Dzida, M., Musiał, M., Zorębski, E., Zorębski, M., Jacquemin, J., Goodrich, P., ... & Paluch, M. (2019). Comparative study of effect of alkyl chain length on thermophysical characteristics of five N-alkylpyridinium bis(trifluoromethylsulfonyl)imides with selected imidazolium-based ionic liquids. Journal of Molecular Liquids, 278, 401-412.

Gartner Group. (2014). Data mining. Retrieved from https://www.gartner.com/en/information-technology/glossary/data-mining#:~:text=Data%20mining%20is%20the%20process,as%20statistical%20and%20mathematical%20techniques.

Ghasemian, E., Zobeydi, R. (2013). Ionic liquids surface tension prediction based on enthalpy of vaporization. Retrieved from https://www-sciencedirect-com.dlsu.idm.oclc.org/science/article/pii/S0378381213004354?via%3Dihub&fbclid=IwAR3OIJALZGBZCyW4rkQnIuDduvQAzV0TvHK_NnSAImvPgGpcvku9eTyw7Ec

Harris, K. R., & Kanakubo, M. (2016). Self-diffusion coefficients and related transport properties for a number of fragile ionic liquids. Journal of Chemical & Engineering Data, 61(7), 2399-2411.

Helmenstine, A. (2020). Understand electrical conductivity. Retrieved from https://www.thoughtco.com/definition-of-electrical-conductivity-605064

Iwasaki, K., Yoshii, K., Tsuda, T., & Kuwabata, S. (2017). Physicochemical properties of phenyl trifluoroborate-based room temperature ionic liquids. Journal of Molecular Liquids, 246, 236-243.

Liu, Q. S., Liu, J., Liu, X. X., & Zhang, S. T. (2015). Density, dynamic viscosity, and electrical conductivity of two hydrophobic functionalized ionic liquids. The Journal of Chemical Thermodynamics, 90, 39-45.

Loginworks Softwares. (2014). Data mining and its importance. Retrieved from https://www.loginworks.com/blogs/217-data-mining-and-its-importance/

Nazet, A., Sokolov, S., Sonnleitner, T., Friesen, S., & Buchner, R. (2017). Densities, refractive indices, viscosities, and conductivities of non-imidazolium ionic liquids [Et3S][TFSI],[Et2MeS][TFSI],[BuPy][TFSI],[N8881][TFA], and [P14][DCA]. Journal of Chemical & Engineering Data, 62(9), 2549-2561.

Nazet, A., Sokolov, S., Sonnleitner, T., Makino, T., Kanakubo, M., & Buchner, R. (2015). Densities, viscosities, and conductivities of the imidazolium ionic liquids

[Emim][Ac],[Emim][FAP],[Bmim][BETI],[Bmim][FSI],[Hmim][TFSI], and [Omim][TFSI]. Journal of Chemical & Engineering Data, 60(8), 2400-2411.

Nazet, A., Weiß, L., & Buchner, R. (2017). Dielectric relaxation of nitromethane and its mixtures with ethylammonium nitrate: Evidence for strong ion association induced by hydrogen bonding. Journal of Molecular Liquids, 228, 81-90.

Oliveira, F. S., Rebelo, L. P., & Marrucho, I. M. (2015). Influence of different inorganic salts on the ionicity and thermophysical properties of 1-ethyl-3-methylimidazolium acetate ionic liquid. Journal of Chemical & Engineering Data, 60(3), 781-789.

Papović, S., Gadžurić, S., Bešter-Rogač, M., & Vraneš, M. (2016). Effect of the alkyl chain length on the electrical conductivity of six (imidazolium-based ionic liquids+ γ-butyrolactone) binary mixtures. The Journal of Chemical Thermodynamics, 102, 367-377.

Sattari, M., Kamari, A., Mohammadi, A., Ramjugernath, D. (2016). On the prediction of critical temperatures of ionic liquids: Model development and evaluation. Retrieved from https://www-sciencedirect-com.dlsu.idm.oclc.org/science/article/pii/S0378381215302302?via%3Dihub&fbclid=IwAR19SbM443XduRS3XtkkwM2YINsmtZJJL_gwmVzVvOB-JGzFqn7hvkWin88

Shakeel, A., Mahmood, H., Ullah, Z., Yasin, S., Iqbal, T., Chassagne, C. & Moniruzzaman, M. (2019). Rheology of pure ionic liquids and their complex fluids: a review. Retrieved fromhttps://pubs.acs.org/doi/abs/10.1021/acssuschemeng.9b02232?fbclid=IwAR1Hw5h12e4_SLADAn3-C1D4783q3qX9DyywvumKun4et-OUMCbUXnjH-tg

Soriano, A., Agapito, A., Lagumbay, L., Caparanga, A., & Li, M. (2010). A simple approach to predict molar heat capacity of ionic liquids using group-additivity method. Journal Of The Taiwan Institute Of Chemical Engineers, 41(3), 307-314. doi: 10.1016/j.jtice.2009.11.003

Valderrama, J. O., Forero, L. A., & Rojas, R. E. (2012). Critical properties and normal boiling temperature of ionic liquids. Update and a new consistency test. Industrial & engineering chemistry research, 51(22), 7838-7844.

Welton, T. (2018). Ionic liquids: a brief history. Biophysical reviews, 10(3), 691-706.

Zhang, Q., Cai, S., Zhang, W., Lan, Y., & Zhang, X. (2017). Density, viscosity, conductivity, refractive index and interaction study of binary mixtures of the ionic liquid 1–ethyl3–methylimidazolium acetate withmethyldiethanolamine. Journal of Molecular Liquids, 233, 471-478.

Zubeir, L. F., Romanos, G. E., Weggemans, W. M., Iliev, B., Schubert, T. J., & Kroon, M. C. (2015). Solubility and diffusivity of CO2 in the ionic liquid 1-butyl-3-methylimidazolium tricyanomethanide within a large pressure range (0.01 MPa to 10 MPa). Journal of Chemical & Engineering Data, 60(6), 1544-1562.

A Preliminary Study on the Chiral Vector Approach in Determining the Optimum Structure of Carbon Nanotubes and its Correlation to the Chemical Potential Energy Using Avogadro

James Harris R. Bajande, Bren Daniel J. Ebriega , Justin Randolph N. Labios, and Mike Lester D. Uy
De La Salle University Integrated School, Manila

Abstract: In this study, the following quantitative properties of carbon nanotubes were explored: the chiral vectors, which are numbers that describe the carbon nanotubes' structure, and properties such as chemical potential energy. The objective of this study is to simulate various carbon nanotube structures with chiral vectors that range from (0-3) and find a relation between these chiral vectors and the chemical potential energy. Using the software Avogadro, 12 carbon nanotubes with different chiral vectors (n, m) were simulated. These carbon nanotubes were of different lengths to keep the number of atoms in the molecules as close to 100 as possible. Avogadro was also used to calculate the theoretical chemical potential energy of these molecules. Using multiple correlation to analyze the simulations' data, an R2 value of 0.632 was obtained, which indicates a small positive linear association between them.

Key Words: carbon nanotubes; chiral vectors; chemical potential energy

1. INTRODUCTION

1.1. Background of the Study

Scientists have been studying carbon nanotubes (CNTs) for the past two decades because of their superior mechanical and electrical properties. In terms of structure, CNTs are a sheet of graphene rolled into a tube. CNTs can be classified as single-walled CNT (SWCNT), double-walled CNT (DWCNT), or multi-walled CNT (MWCNT), depending on the number of carbon-layers in their sidewalls (Schnorr & Swager, 2011).

An SWCNT is a hollow cylinder made up of covalently bonded carbon atoms arranged in a hexagonal pattern. Because of its atomic structure and unique carbon bond properties, the SWCNT has remarkable mechanical and electrical properties (Gao et al., 2021).

Additionally, different types of SWCNTs can be identified, except for their length, by the orientation of the tube axis relative to the carbon network. They are represented by the indices of their chiral vector, n and m (Schnorr & Swager, 2011). The CNT is an armchair when the chiral indices, n and m, are equal. On the other hand, the CNT is zigzag when either n or m is 0. Moreover, the CNT is chiral when their chiral indices are neither of these two (Kaushik & Majumder, 2015). Depending on their composition, CNT may also have metallic or semiconducting properties. The CNT is metallic if n - m = 3q (where q is an integer and n>m) and semiconducting if not (J. Liu et al., 2017). The n and m integers precisely define nanotube chirality and specify the electronic band structure. Hence, the chirality of carbon nanotubes has a significant impact on their electronic properties (Tune et al., 2012).

Further studies show that CNTs have received much interest because they are great at lowering resistance and improving the electrochemical efficiency of composite cathodes (Qin et al., 2014), which is the positive electrode of a battery (Battery University, 2020). Moreover, incorporating CNT into sulfur cathode gives rise to advanced electrodes with improved discharging capacity and cycling performance (L. Zhu et al., 2014).

Furthermore, as seen in batteries and electrochemical pseudocapacitors, energy storage technologies are based on the conversion of chemical potential energy to electrical energy, with the energy being stored in the form of chemical potential energy (C. Liu et al., 2016), which is the energy stored in the chemical bonds of a substance that can be absorbed or released due to a change of the particle number of the given species (CK-12 Foundation, 2021).

Consequently, in this study, the researchers focused on the SWCNT's structure, chiral vectors, and chemical potential energy.

Based on existing literature, no studies have been found regarding the use of virtual simulation to investigate the chemical potential energy of a CNT. Furthermore, no studies have been found describing the effects of changing a CNT's chiral vectors to its chemical potential energy. Despite the lack of existing studies, a molecular editor helped gather the necessary data in this research. Avogadro by

Avogadro Chemistry was the molecular editor used in this study.

This study aims to fill the gap in analyzing the relationship between chiral vectors and the chemical potential energy of CNTs, as this has not been determined in the existing literature. The study would enable future researchers to better determine the optimal CNT structure in possible energy-related applications such as battery electrodes (X. Liu et al., 2012).

1.2 Research Objective

This paper's main objective is to simulate a carbon nanotube structure using different chiral vectors to find a carbon nanotube structure that will yield the highest chemical potential energy with the same number of atoms. Existing literature was the basis for finding the optimal structure. Furthermore, the study aims to determine the relationship between the structures and the chemical potential energy.

1.2.1 Specific Objectives

a. To accomplish this task, the researchers aim to do the following:
b. Find the chiral vectors and make the pairings needed in building the CNT structure with a set number of 100 atoms
c. Simulate different carbon nanotube structures with varying chiral vectors and get their chemical potential energy
d. Sort data according to the structure that has the highest energy
e. Use correlation to figure out the relationship between the chiral vectors and the energy

1.3 Scope and Limitations

This research was limited to only SWCNT structures as their electrical properties are significantly higher than those of (MWCNTs) (Zaytseva & Neumann, 2016). In addition to having a simpler structure and higher electrical characteristics than MWCNTs, SWCNTs are the most studied classification of CNTs both experimentally and theoretically (Laird et al., 2015). As this research was limited to single-walled carbon nanotubes, the researchers did not tackle the effects of varying numbers of walls. Moreover, the number of atoms was only normalized to see if a structure change was the cause and not the size of the molecules increasing. Hence, the researchers have limited the CNT's structure to have only 100 atoms each or 102 if 100 is not possible. Lastly, chiral values used were only from a range of 0-3.

1.4 Significance of the Study

This study contributes to the body of knowledge regarding carbon nanotubes' structures and their implications about their chemical potential energy that may be converted into other forms of energy, such as electrical energy. With the growing need for sustainable energy, this research may serve as a constituent in further research applying carbon nanotubes into batteries. In turn, this study could hopefully reveal new ways to use carbon nanotubes as a material viable for sustainable energy. The data and information gathered can also provide additional resources for future researchers. Furthermore, using simulation prevents unnecessary effort and laborious work. Lastly, since the simulation is in a virtual environment, it is cheaper and requires lesser materials and equipment than actual laboratory work.

2. METHODOLOGY

2.1. Research Design

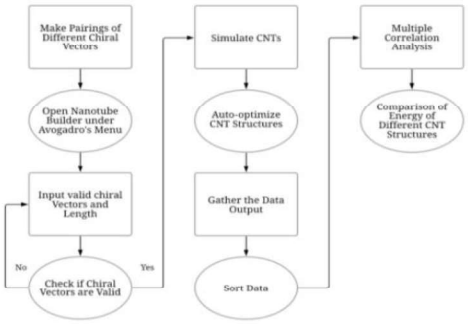

Figure 1. *Flowchart of Methodology*

Figure 1 was used as the flowchart for the entire methodology. The researchers have chosen Avogadro as the visualizer and simulator for the experiment, based on Hanwell et al. (2012). The virtual carbon nanotube (CNT) was built with varying chiral vector and length values using the "Nanotube Builder" available in Avogadro. This option was accessed through the "Build Menu" found in the Toolbar. The builder takes in input for chiral vectors n and m as well as length. The researchers tested different combinations of chiral vectors and length values using different CNT shapes as some chiral vector pairings are not possible.

This study made use of quantitative data, which was collected from Avogadro. After the researchers inputted the chiral vectors n and m, the output was three different types of CNT structures: zigzag, armchair, and chiral. After the CNTs were built, they used Avogadro's auto-optimization, which automatically optimized the CNT's geometry according to the inputted values of chiral vectors and

length. The final output was the final structure of the base CNT and its chemical potential energy.

The researchers only used Avogadro and had no other participants aside from themselves. Furthermore, the researchers only used the simulator mentioned above and mathematical means and tools to acquire their data. Thus, no ethical issues were violated in this study.

2.2. Data Collection Method

The primary data collected were the carbon nanotubes' structures based on the manipulated chiral vectors and the chemical potential energy produced that was determined by the CNT structure. The data was collected from the various simulations that were run in Avogadro. Each simulation had different chiral vector pairs (n,m). These values were selected by choosing a maximum value for the chiral vectors and producing every possible carbon nanotube with chiral vector values less than or equal to the chosen value. In this case, the chosen value was 3, which theoretically gives 16 different (n,m) pairs. However, there are certain (n,m) pairs that are not possible, these being (0,0), (0,1), (1,0), and (1,1). This is because either n or m has to be greater than 1. With this limitation in mind, 12 carbon nanotubes were simulated: (0,2), (0,3), (1,2), (1,3), (2,0), (2,1), (2,2), (2,3), (3,0), (3,1), (3,2), and (3,3), with the lengths modified to keep the number of atoms in the carbon nanotubes as close to 100 as possible to normalize the data as best as possible. After each simulation, the carbon nanotubes' geometries were further optimized. Once these geometries were as optimized as the software would allow, Avogadro automatically calculated and displayed the theoretical chemical potential energy (kJ/mol) produced by the setup.

Energy output in Avogadro's "Calculate Energy" is computed by a variation of the "force field," called Merck Molecular Force Field or MMFF94. MMFF94 is designed to deal with condensed-phase processes in molecular dynamics simulation and molecular geometry optimization in proteins and other biological systems (H. Zhu, 2014).

Avogadro uses the variant MMFF94s (Cornell & Hutchison, 2015). The "s" stands for static as this variant is better suited for time-averaged static molecular geometry (H. Zhu, 2014).

All simulations were done using an AMD Ryzen 5 3550H CPU, Nvidia GeForce GTX 1650 GPU, and 16GB of DDR-2400 RAM.

2.3 Data Collection Instruments

Avogadro is a free, open-source, and cross-platform molecule editor developed by Avogadro Chemistry. The program is written in C++, but Python scripts can be used as extensions to add functionality. Avogadro supports multithreading for rendering and computation, which can reduce wait times on processors with multiple cores. However, GPUs cannot be used for hardware acceleration (Hanwell et al., 2012).

Avogadro has a robust feature set that allows it to create many different types of molecules, including a Nanotube Builder that can create different nanotubes depending on the parameters. It can also optimize molecules' geometry through the Optimize Geometry tool, which gives proper bond angles and lengths. The Auto Optimize tool also does this but continuously. Lastly, it can also calculate the energy of a system through its Calculate Energy function (Cornell & Hutchison, 2015).

2.4 Data Analysis

After collecting data, the researchers analyzed the chiral vectors used in creating the structure and energy produced by the carbon nanotubes and the structure of the CNT that was determined by the chiral vector. A chiral vector pair vs. energy graph was created to easily visualize the trend between the two variables and compare the difference in the energy output of different chiral vector pairs. The statistical tool used was a multiple correlation between the chemical potential energy and the chiral vectors that affect the structure of the CNT structure. A corresponding scatter plot was also used to visualize further the correlation between the two chiral vectors and energy. The unstandardized predicted value of the energy was used to account for the two chiral vectors, the independent variables. This was then plotted against the energy to create the scatter plot. The unstandardized predicted value was calculated after the equation of the line was determined since it is the value that the model predicted for the dependent variables (Penn State Eberly College of Science, 2018). To do this, the researchers opted to use Microsoft Excel and IBM SPSS Statistics to help analyze their data.

3. RESULTS AND DISCUSSION

3.1 Simulation Results

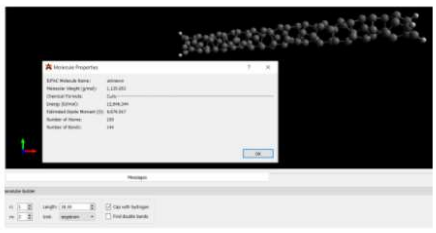

Figure 2. *CNT with chiral vectors (1,2)*

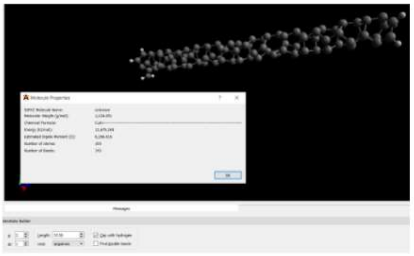

Figure 3. *CNT with chiral vectors (2,1)*

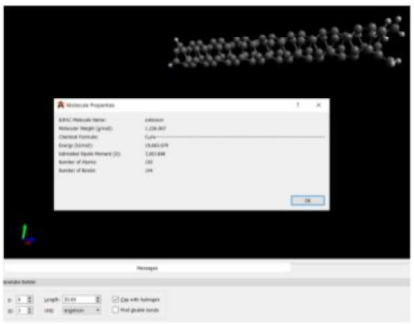

Figure 4. *CNT with chiral vectors (0,3)*

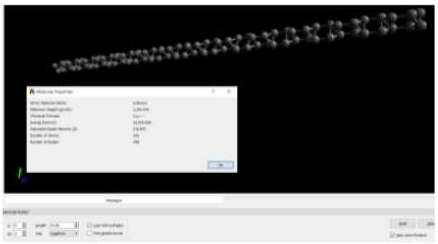

Figure 5. *CNT with chiral vectors (0,2)*

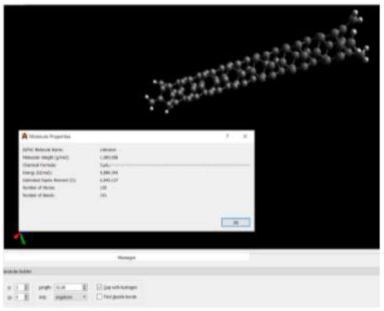

Figure 6. *CNT with chiral vectors (3,0)*

Figure 7. *CNT with chiral vectors (2,0)*

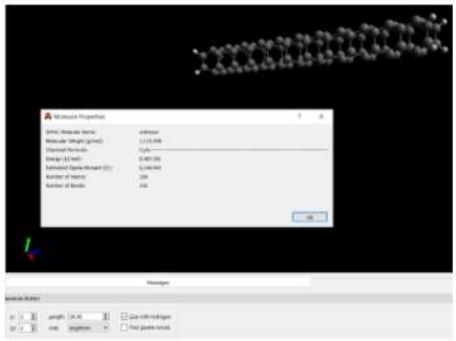

Figure 8. *CNT with chiral vectors (2,2)*

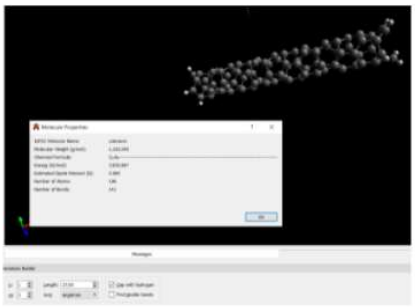

Figure 9. *CNT with chiral vectors (1,3)*

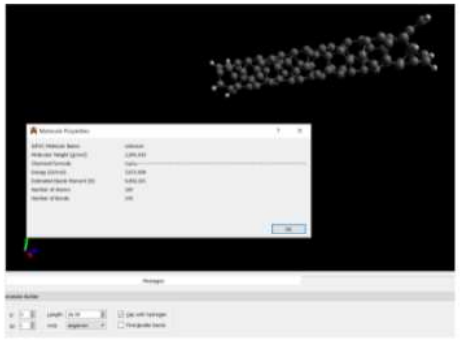

Figure 10. *CNT with chiral vectors (3,1)*

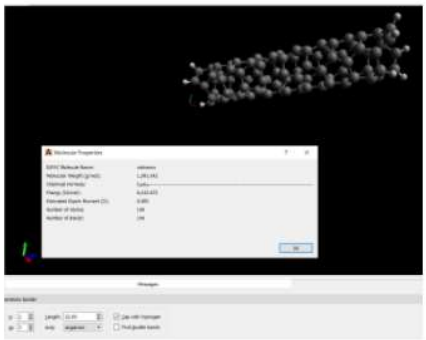

Figure 11. *CNT with chiral vectors (2,3)*

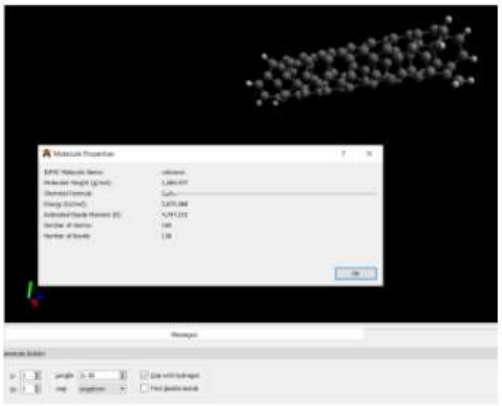

Figure 12. *CNT with chiral vectors (3,2)*

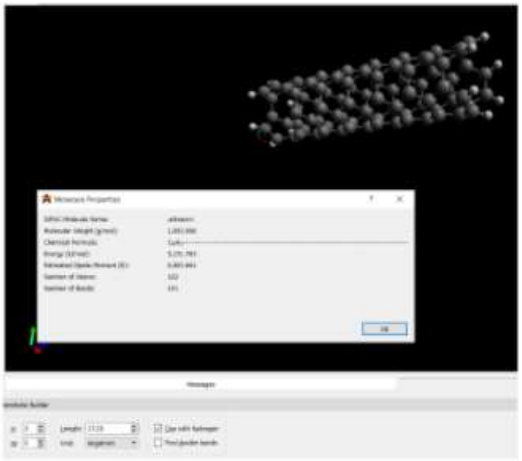

Figure 13. *CNT with chiral vectors (3,3)*

Figures 2-13 show each simulation of CNT with data regarding chiral vectors n and m, classification, number of atoms, number of bonds, CNT length (angstrom), molecular weight (g/mol), and chemical potential energy (kJ/mol). The structures are all set to 100 atoms except for some structures that have 102 because, as explained before, the next shortest value would be 96.

3.2 Primary observations

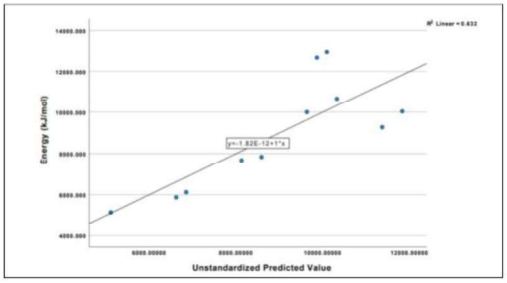

Figure 15. *Linear regression of Energy vs. Unstandardized Predicted Value*

In Table 1, the information about the CNTs with different structures and chiral vectors is displayed.

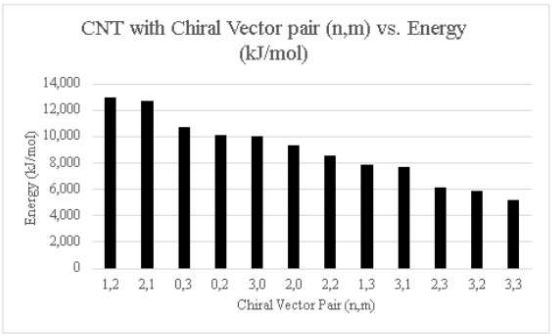

Figure 14. *Bar graph comparing the energy values of each CNT*

In previous research by Jing Liu et al. (2017), it was stated that CNTs that follow the trend of n - m = 3q, where q is an integer, are the most conductive while others are only semiconductive.

It can be seen in Figure 14 that two of the simulated CNTs were chiral and have the most energy, given that they have the same number of atoms. CNTs with (1,2) and (2,1) yield 12,946.344 kJ/mol and 12,675.248 kJ/mol respectively. These CNTs do not follow the trend indicated by the previous research in the previous paragraph. They both exceed two thousand kJ/mol more than the third-highest energy CNT, the (0,3). Moreover, it can be seen that different CNT structures produce different energy outputs, especially with the two armchair structures that have a difference of 3335.618 kJ/mol even though they have the same structure and the same number of atoms. Lastly, there is no obvious pattern that can be seen in the produced data. As the CNTs were made to have 100 atoms, with a few exceptions, it can be seen that the number of bonds, length, molecular weight, and energy are very different from one another and do not follow a specific trend.

3.3 Statistical Analysis

Figure 15 shows the scatter plot corresponding to the correlation between the two chiral vectors and the energy. The y-axis represents chemical potential energy (dependent variable), while the x-axis represents the two chiral vectors (independent variable). The dependent variable's unstandardized predicted value was used to account for the two independent variables and was plotted against the dependent variable. This produced an R2 value of 0.632, consistent with the R2 value in Table 2.

This R2 value of 0.632 is positive, which shows a small positive linear association between them (Kiernan, 2014).

4. CONCLUSIONS

Chiral vectors that range from (0-3) were paired up and used to make carbon nanotubes. Using the software Avogadro, only 12 carbon nanotubes with different chiral vectors were simulated successfully, which are (0,2), (0,3), (1,2), (1,3), (2,0), (2,1), (2,2), (2,3), (3,0), (3,1), (3,2), and (3,3). Since CNTs can only be made if one chiral vector is at least greater than 1, chiral vector pairs (0,0), (0,1), (1,0), and (1,1) are not possible inputs to create a CNT. Results were then sorted with the CNT, with the highest amount of energy being the first. Chiral CNTs with (1,2) and (2,1) yielded the highest energy of 12,946.344 kJ/mol and 12,675.248 kJ/mol, respectively. Using multiple correlation to analyze the simulations' data, an R^2 value of 0.632 was obtained, which indicates a small positive linear association between them.

In conclusion, this study showed the relationship between the chiral vectors and the chemical potential energy of CNTs. Further simulations can be made by identifying other structures not limited to CNTs. Another recommendation is to obtain the average for each structure and compare it to other literature on what applications it can be utilized.

5. ACKNOWLEDGMENTS

First and foremost, the researchers would like to express their deepest gratitude and most tremendous appreciation to the following persons who helped and guided them through the project. The researchers would like to thank Dr. Archie Maglaya, Sir Melchizedek Alipio, and Dr. Gil Nonato Santos, Ph.D., the research advisors who helped the researchers in the first part of their project and in polishing the paper. The researchers thank Ms. Liezl Rillera - Astudillo, the research coordinator, for guiding them in their research project's makings. The researchers thank the previous researchers who have conducted the necessary research for this research to be possible. Moreover, the researchers thank De La Salle University for allowing the researchers to fulfill this study and supporting them financially. The researchers express their gratitude to the parents, who constantly give them motivation and support them in any way possible. Lastly, the researchers thank the almighty God, who gave them the knowledge and courage to fulfill this research leading them to the right path.

6. REFERENCES

Battery University. (2020, November 20). BU-104b: Battery Building Blocks – Battery University. Batteryuniversity.com. https://batteryuniversity.com/learn/article/bu_104b_building_blocks_of_a_battery

CK-12 Foundation. (2021). CK12-Foundation. CK-12 Foundation; CK-12 Foundation. https://flexbooks.ck12.org/cbook/ck-12-chemistry-flexbook-2.0/section/17.1/primary/lesson/chemical-potential-energy-chem

Cornell, T., & Hutchison, G. (2015). Learning Avogadro The Molecular Editor. Wustl.edu. https://dasher.wustl.edu/chem430/software/avogadro/learning-avogadro.pdf

Gao, M., Bian, L., & Liang, X. (2021). Analysis for thermal properties and some influence parameters on carbon nanotubes by an energy method. Applied Mathematical Modelling, 89, 73–88. https://doi.org/10.1016/j.apm.2020.07.041

Hanwell, M. D., Curtis, D. E., Lonie, D. C., Vandermeerschd, T., Zurek, E., & Hutchison, G. R. (2012). Avogadro: An advanced semantic chemical editor, visualization, and analysis platform. Journal of Cheminformatics, 4(8). https://doi.org/10.1186/1758-2946-4-17

Kaushik, B. K., & Majumder, M. K. (2015). Carbon nanotube based VLSI interconnects: Analysis and design. SpringerBriefs in Applied Sciences and Technology, 9788132220466, i–iv. https://doi.org/10.1007/978-81-322-2047-3

Kiernan, D. (2014, January 16). Chapter 7: Correlation and Simple Linear Regression. Geneseo.edu; Open SUNY Textbooks. https://milnepublishing.geneseo.edu/natural-resources-biometrics/chapter/chapter-7-correlation-and-simple-linear-regression/

Laird, E. A., Kuemmeth, F., Steele, G. A., Grove-Rasmussen, K., Nygård, J., Flensberg, K., & Kouwenhoven, L. P. (2015). Quantum transport in carbon nanotubes. Reviews of Modern Physics, 87(3), 703–764. https://doi.org/10.1103/RevModPhys.87.703

Liu, C., Neale, Z. G., & Cao, G. (2016). Understanding electrochemical potentials of cathode materials in rechargeable batteries. Materials Today, 19(2),

109–123. https://doi.org/10.1016/j.mattod.2015.10.009

Liu, J., Lu, J., Lin, X., Tang, Y., Liu, Y., Wang, T., & Zhu, H. (2017). The electronic properties of chiral carbon nanotubes. Computational Materials Science, 129, 290–294. https://doi.org/10.1016/j.commatsci.2016.12.035

Liu, X. M., Huang, Z. dong, Oh, S. woon, Zhang, B., Ma, P. C., Yuen, M. M. F., & Kim, J. K. (2012). Carbon nanotube (CNT)-based composites as electrode material for rechargeable Li-ion batteries: A review. Composites Science and Technology, 72(2), 121–144. https://doi.org/10.1016/j.compscitech.2011.11.019

Penn State Eberly College of Science. (2018). 2.1 - What is Simple Linear Regression? | STAT 462. Psu.edu. https://online.stat.psu.edu/stat462/node/91/

Qin, G., Ma, Q., & Wang, C. (2014). A porous C/LiFePO4/multiwalled carbon nanotubes cathode material for Lithium ion batteries. Electrochimica Acta, 115, 407–415. https://doi.org/10.1016/j.electacta.2013.10.177

Schnorr, J. M., & Swager, T. M. (2011). Emerging applications of carbon nanotubes. Chemistry of Materials, 23(3), 646–657. https://doi.org/10.1021/cm102406h

Tune, D. D., Flavel, B. S., Krupke, R., & Shapter, J. G. (2012). Carbon nanotube-silicon solar cells. Advanced Energy Materials, 2(9), 1043–1055. https://doi.org/10.1002/aenm.201200249

Zaytseva, O., & Neumann, G. (2016). Carbon nanomaterials: Production, impact on plant development, agricultural and environmental applications. Chemical and Biological Technologies in Agriculture, 3(1), 1–26. https://doi.org/10.1186/s40538-016-0070-8

Zhu, H. (2014, April 28). Implementation and application of the MMFF94 force field. Unl.edu. https://digitalcommons.unl.edu/cgi/viewcontent.cgi?article=1047&context=chemistrydiss

Zhu, L., Zhu, W., Cheng, X. B., Huang, J. Q., Peng, H. J., Yang, S. H., & Zhang, Q. (2014). Cathode materials based on carbon nanotubes for high-energy-density lithium-sulfur batteries. Carbon, 75, 161–168. https://doi.org/10.1016/j.carbon.2014.03.049

The Effect of Coconut Fiber as Concrete Reinforcement on Abrasion Resistance and Water Permeability

Karl Andre F. Aquino, Marie Bernadette B. Lasay, Jesus E. Acuña,
and Armaine Lizbeth B. Herbon
De La Salle University Integrated School, Biñan City, Laguna

Abstract: The quality of infrastructure in the Philippines is one of the lowest amongst its neighboring countries. This is affected by the materials used in construction such as concrete. The mechanical and durability properties of concrete can be improved with fiber reinforcements. Coconut fiber is known to be the most ductile from all natural fibers, and the Philippines is a major producer of coconut. The study aims to determine the effect of coconut fiber on concrete reinforcement by examining its abrasion resistance and water permeability. The samples were cured for 28 days after setting and subjected to abrasion resistance and water permeability tests. The abrasion resistance decreased with higher fiber content; however, fiber content equal to or lower than 2.5% had higher resistance as compared to normal concrete. The water permeability of samples increased along with the coconut fiber content, with a significant increase observed in fiber contents equal to above 5%. The best overall results were achieved with CFRC containing 2.5% fiber content.

Key Words: concrete; coconut fiber; abrasion resistance; water permeability

1. INTRODUCTION

Infrastructures in the Philippines are mostly outdated and lacking. According to IMF Focus (2020), the Philippines, in terms of infrastructure quality, is below most of the other neighboring countries. As the Philippines plan on increasing its budget allocated to public infrastructure with the Build, Build, Build program, their aim is to improve the overall quality to lessen the impact of climate-related disasters.

According to Burton (2018), the Philippines is the second-largest producer of Cocos nucifera or coconut in the world, producing over 150 million tons of coconut with a quarter of its total farmland dedicated to coconut production. However, the percentages of husk utilization for coir production in the three major islands of the Philippines are all below 55%, with more than 45% of the coconut husks produced are unutilized (Pogosa et al., 2018).

Copious studies concerning the mechanical properties of coconut fiber as concrete reinforcement are already evident. As exhibited in the paper of Onuaguluchi & Banthia in 2010, there are yet more studies to determine the durability properties of the said fiber (i.e., abrasion resistance and water permeability). Thus, this research focused on the stated durability properties of coconut fiber-reinforced concrete (CFRC).

According to Aziz in 1981, other well-known natural fiber reinforcements (e.g., sisai, sugarcane bagasse, bamboo, juta, wood, akwara, elephant grass, water-reed, plantain, and musamba) are heavily used and ensure many benefits (i.e., improved tensile and compressive strength, post cracking resistance, high energy absorbing characteristics and fatigue strength). However, in comparison to all natural fibers, coconut fiber is reaffirmed to be the most ductile (Aditya, Anushree, Varghese, & Antony, 2015).

This study aims to produce CFRC containing 0%, 2.5%, 5%, 7.5% coconut fiber content by weight which was to be cured for 28 days. The samples were then tested to assess the durability of CFRC in terms of abrasion resistance and water permeability.

2. METHODOLOGY

2.1. Materials

The chemicals used were silica fume for durability and superplasticizer as a high range water reducer. The equipment used are as follows: (a) the Belt Sander from Black+Decker Model DS321; (b) the Digital Weighing Scale Model SF-400; (c) the Digital Kitchen Scale from KONCO, which was used for obtaining specific measurements; and (d) a sieve mesh, which is a mesh made of metal, fiber, or cloth, assembled to provide defined opening. The raw materials used for the mixture were Type 1 Portland cement from CEMEX, gravel, sand, drywall, wood planks, and coconut fiber. The coconut fiber was treated by first cleaning it with water; then, it was subjected to 200° C in an oven for 30 min or until constant weight is attained.

2.2. Research Design

In this study, the researchers aimed to answer whether coconut fiber reinforcement can affect the abrasion resistance and water permeability of concrete as well as which amount would yield the best results. A total of 24 rectangular slab samples with dimensions 120 x 70 x 50 mm were made and cured for 28 days. The samples were labeled as shown in Table 1. There were two experimental setups prepared: the abrasion resistance test setup and the water permeability test setup.

Table 1. *ID and quantity of samples*

Sample ID	Description	Quantity
CFRC-0	Control concrete samples with 0% fiber content	6
CFRC-2.5	CFRC samples with 2.5% fiber content	6
CFRC-5	CFRC samples with 5% fiber content	6
CFRC-7.5	CFRC samples with 7.5% fiber content	6

2.3. Concrete Samples

The ratio for the materials used in the mixture were 2.60:3.90: 3.90:0.90:0.26:0.03 for the mixing of cement, sand, gravel, water, silica fume, and superplasticizer. The mixture ratio was based on the study of Ahmad et al. (2020) wherein they have improved the mechanical properties of concrete with the use of coconut fiber as reinforcement. The mixture was cast in a 120 x 70 x 50 mm concrete mold made from drywall; a diagram of the mold is shown in Figure 1. After setting, it was removed from the mold and cured for a minimum of 28 days. A total of 24 concrete blocks were prepared to conduct the abrasion resistance and water permeability tests.

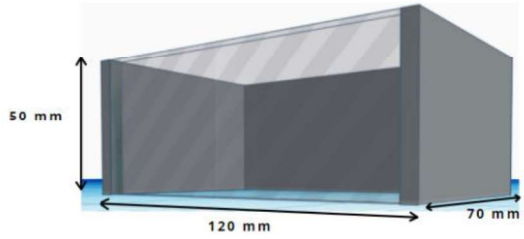

Figure 1. *Diagram of Mold Dimensions*

2.4. Sample Testing

Figure 2 shows the experimental setup for the abrasion resistance test based on the test method coming from the American Society of Testing and Materials (ASTM), specifically ASTM C779 Method A (Kumar & Sharma, 2014). It is an alternative method of testing devised from ASTM C779 wherein a constantly rotating abrasive surface is applied on the sample using a belt sander with wood planks used as support. It utilizes the wood planks as support for the sample and the belt sander to abrade the surface. The weight of the samples at intervals of 0 min, 5 min, 10 min, and 15 min as well as the cross-section of the samples were observed.

Figure 2. *Abrasion Resistance Test Setup*

Figure 3 shows the experimental setup for the water permeability test based on ASTM C642-06. The setup is based on ASTM C642-06 wherein the samples are required to be a minimum of 350 cm3 and dried in an oven at 200°C for a minimum of 45 minutes or until constant weight is attained. The samples were then submerged for intervals of 0 h, 0.5 h, and 72 h wherein the weight was recorded. The volume of permeable voids (Pv%) was then calculated with the formula provided in ASTM C642-06, Pv% = (Wf - Wi)Wf 100, wherein Wi is the initial weight, and Wf is the final weight of the sample.

Figure 3. *Water Permeability Test Setup*

3. RESULTS AND DISCUSSION

3.1 Abrasion Resistance

Abrasion resistance (AR) of concrete can determine its survivability in abrasive environments. During the AR test, all samples exhibited no loss in their height. Furthermore, in the sample with the highest percentage, larger cracks and holes can be found within the cross-section of the concrete, which is displayed in Figure 4. The weight of the samples in all intervals is shown in Figure 5.

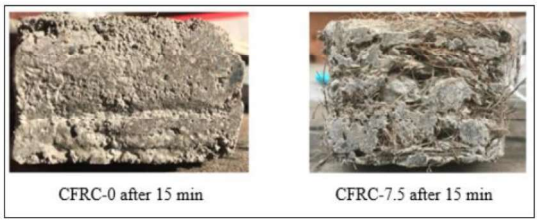

Figure 4. *A comparison of the cross-section of CFRC-0 and CFRC-7.5*

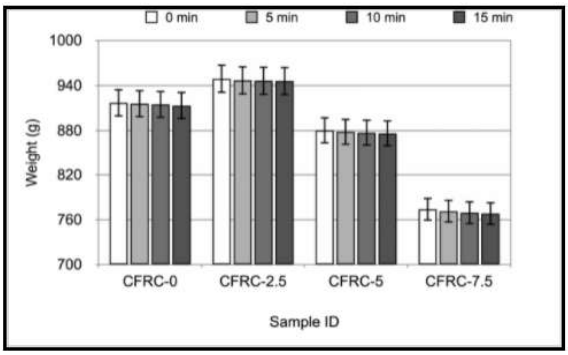

Figure 5. *Avg. weight at intervals during AR tests*

Figure 6 shows the average weight loss, initial weight - final weight, during the abrasion resistance test for each of the samples. The data shows that the highest fiber content, i.e., 7.5%, also had the most total weight difference amongst all samples, which suggests that it is the least resistant amongst all samples. Furthermore, all CFRC samples observed a lower resistance during the first 5 min, having the most weight loss whilst it diminishes as it is exposed to abrasion for longer periods of time. However, the control samples observed a constant loss in weight after each interval. Hence, the said observation asserts that the fiber content of CFRC has an inverse relationship with its abrasion resistance.

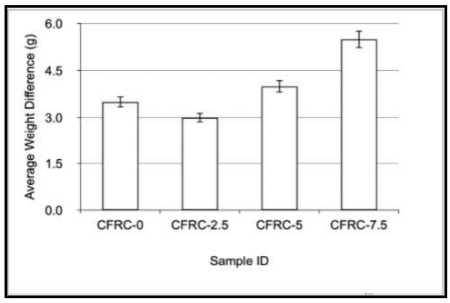

Figure 6. *Avg. weight difference of all samples after AR test*

3.2 Water Permeability

The water permeability (WP) of concrete can affect its durability as higher rates of absorption will allow molecules to make the structure unstable, whilst lower rates would mean a stronger resistance against fluids. These rates are affected by the volume of permeable voids an object has. Figure 7 shows the average weight of the samples in each interval from 3 trials of the WP test. There was a significant weight difference among samples of the same type. These may be due to the inconsistency of pouring the mixture during molding and casting. As shown in Figure 7, all samples showed a significant increase in weight during the first 30 min of water submersion. After 72 h, the weight of all samples showed a smaller increase as compared to the first 30 min.

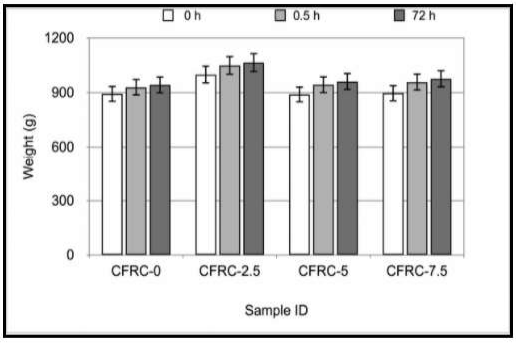

Figure 7. *Avg. weight at intervals during WP tests*

The results show that samples with higher fiber content have a higher percentage of permeable voids, refer to Figure 8. These are similar to those from the study of Rao et al. (2015), wherein concrete with coconut shell aggregate added to its mixture showed a higher volume of permeable voids as compared to normal concrete. The higher percentage indicates that the water absorption rate also increases along with fiber content. Thus, the fiber content should not increase by 2.5% fiber content. The samples CFRC-5 and CFRC-7.5 are more susceptible to internal damage while CFRC-2.5 only has a slight increase in permeable voids as compared to the CFRC-0. Figure 8 shows the general increase in permeable voids as the fiber content increases.

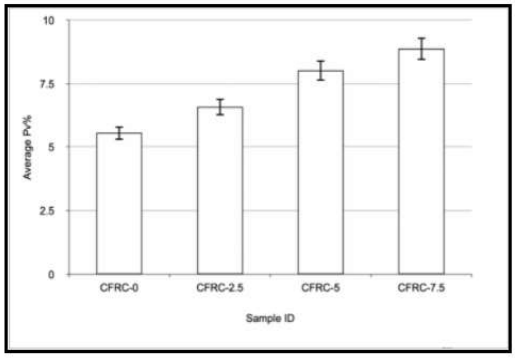

Figure 8. *Permeable voids in samples*

The significant increase in the volume of permeable voids on samples with more than 2.5% fiber content indicates that the reinforcement of concrete with coconut fibers should be no more than 2.5%. According to Ahmad et al. (2015), the CFRC with 1.5% fiber content provided the best results in terms of mechanical properties, and they have also stated that any more than that showed fewer improvements.

4. CONCLUSIONS

The study has shown the effects of coconut fiber as concrete reinforcement. In the abrasion resistance test, the findings suggest that high fiber content leads to lower abrasion resistance. The data also asserted that CFRC can withstand abrasive environments in longer time intervals since its abrasion resistance increases over time unlike the control sample. Thus, it is recommended that the fiber content of the CFRC must stay within 2.5% to ensure the highest abrasion resistance of the sample. Furthermore, in the water permeability test, the results suggest that fiber content less than 2.5% is recommended as it will decrease the risk of damage and be more effective. Overall, the reinforcement of concrete with coconut fibers at 2.5% fiber content or lower will improve abrasion resistance whilst avoiding major increase in permeable voids. With that said, it is recommended for future research to focus on the proper mixing and curing processes for CFRC along with the placement and orientation of fibers during its production as means to lessen the cracks and voids found within the concrete.

5. ACKNOWLEDGMENTS

The researchers would like to thank their research adviser Dr. Kerry P. Cabral for the guidance and help throughout the research process..

6. REFERENCES

Aditya, T., Anushree, S., Varghese, D. & Antony, J. (2015). Coconut Fibre - A Versatile Material and its Applications in Engineering. Main Proceedings ed. https://doi.org/10.1.1.823.5053

Ahmad, W., Farooq, S. H., Usman, M., Khan, M., Ahmad, A., Aslam, F., Yousef, R. A., Abduljabbar, H. A. & Sufian, M. (2020). Effect of Coconut Fiber length and Content on Properties of High Strength Concrete. Main Proceedings ed. https://doi.org/10.1.1.823.5053

Ali, M., Liu, A., Sou, H. & Chouw, N. (2012). Mechanical and dynamical properties of coconut fiber reinforced concrete. Construction on and Building Materials, 30, 814-825. https://www.academia.edu/17539220/Mechanical_and_dynamic_properties_of_coconut_fiber_reinforced_concrete

ASTM C642-06. (n.d.). Standard Test Method for Density, Absorption, and Voids in Hardened Concrete. ASTM International. ftp://ftp.ecn.purdue.edu/olek/PTanikela/To%20Prof.%20Olek/ASTM%20standards/Density%20absorption%20and%20voids%20in%20hardened%20concrete%20C%20642.pdf

Aziz, M. A., Paramasivam, P., & Lee, S. L. (1981). Prospects for natural fibre reinforced concretes in construction. International Journal of Cement Composites and Lightweight Concrete, 3(2), 123–132. doi:10.1016/0262-5075(81)90006-3

Balakrishna, M. N., Mohamad, F., Evans, R. & Rahman, M. M. (2019). Assessment of water absorption of concrete by Initial surface absorption test. https://www.researchgate.net/publication/330597539_Assessment_of_water_absorption_of_concrete_by_Initial_surface_absorption_test

Burton, J. (2018). The World Leaders in Coconut Production. https://www.worldatlas.com/articles/the-world-leaders-in coconut-production.html

IMF Country Focus. (2020). The Philippines: A Good Time to Expand the Infrastructure Push. https://www.imf.org/en/News/Articles/2020/02/06/na020620the-philippines-a-good-time-to-expand-the-infrastructure-push

Kumar, G. B. R. & Sharma, U.K. (2014). Standard Test Methods for Determination of Abrasion

Resistance of Concrete. International Journal of Civil Engineering Research, 5(2), 15-162. https://www.ripublication.com/ijcer_spl/ijcerv5n2spl_09.pdf

Lee, K. (2017). The Philippines: Infrastructure Opportunities and Challenges. https://hkmb.hktdc.com/en/1X0ABULX/hktdc-research/The-Philippines-Infrastructure-Opportunities-and-Challenges

Onuaguluchi, O., & Banthia, N. (2016). Plant-based natural fibre reinforced cement composites: A review. Cement and Concrete Composites, 68, 96–108. doi:10.1016/j.cemconcomp.2016.02.014

Pogosa, J. O., Asio, V. B., Bande, M. M., Bianchi, S., Pichelin, F. & Grenz, J. (2018). Productivity and Sustainability of Coconut Production and Husk Utilization in the Philippines: Coconut Husk Availability and Utilization. International Journal of Environmental and Rural Development, 9(1), 31-35. https://www.researchgate.net/publication/332259191_Productivity_and_Sustainability_of_Coconut_Production_and_Husk_Utilization_in_the_Philippines_Coconut_Husk_Availability_and_Utilization

Rao, K. V., Swaroop, A. H. L., Rao, P. K. R. & Bharath, C. N. (2015). Study on strength properties of coconut shell concrete. International Journal of Civil Engineering and Technology, 6(3), 42-61. http://www.iaeme.com/MasterAdmin/uploadfolder/IJCIET_06_03_005/IJCIET_06_03_005.pdf